CRYSTAL GROWTH & DESIGN

Article

pubs.acs.org/crystal

Self-Assembly of a Family of Isopolytungstates Induced by the Synergistic Effect of the Nature of Lanthanoids and the pH Variation in the Reaction Process: Syntheses, Structures, and Properties

Hailou Li,[†] Wen Yang,[†] Xiuhua Wang,[†] Lijuan Chen,*[,†] Jianru Ma,[‡] Liwei Zheng,[§] and Junwei Zhao*[,†]

[†]Henan Key Laboratory of Polyoxometalate Chemistry, Institute of Molecular and Crystal Engineering, College of Chemistry and Chemical Engineering, Henan University, Kaifeng, Henan 475004, People's Republic of China

[‡]Anyang Environmental Protection Burea, Anyang, Henan 455000, People's Republic of China

[§]Bruker (Beijing) Scientific Technology Co. Ltd., 11 Zhong Guan Cun Street, Beijing 100081, People's Republic of China

Supporting Information

ABSTRACT: Three types of new lanthanoid(Ln)-containing isopolyoxotungstates $[H_2N(CH_3)_2]_6Na_6[Ln_4(H_2O)_{22}W_{28}O_{94}H_2]_2{\cdot}113H_2O$ [Ln = Pr^{3+} (**1**), Nd^{3+} (**2**), Sm^{3+} (**3**)], $Na_2[Eu(H_2O)_7]_2[Eu(H_2O)_5]_2[W_{22}O_{74}H_2]{\cdot}20H_2O$ (**4**), and $Na_3H_2[Ln(H_2O)_4][Ln(H_2O)_5]_2[W_{22}O_{74}H_2]{\cdot}36H_2O$ [Ln = Gd^{3+} (**5**), Tb^{3+} (**6**), Er^{3+} (**7**), Tm^{3+} (**8**), Yb^{3+} (**9**), Lu^{3+} (**10**)] have been obtained by reacting $Na_2WO_4{\cdot}2H_2O$ with $Ln(NO_3)_3{\cdot}6H_2O$ in the presence of dimethylamine hydrochloride in the acidic aqueous solution and structurally characterized by elemental analyses, IR spectroscopy, UV spectroscopy, electrospray ionization mass spectrometry (ESI–MS), thermogravimetric (TG) analyses, and single-crystal X-ray diffraction. **1**, **2**, and **3** are isostructural and display a one-dimensional (1-D) chain-like alignment built by hexameric Ln_8-comprising $[Ln_4(H_2O)_{22}W_{28}O_{94}H_2]_2^{12-}$ entities via $[Ln(H_2O)_5]^{3+}$ connectors. The $[Ln_4(H_2O)_{22}W_{28}O_{94}H_2]_2^{12-}$ entity consists of two $[Ln_4(H_2O)_{22}W_{28}O_{94}H_2]^{6-}$ subunits connected by two W–O–Ln–O–W linkers. Intriguingly, the rare λ-shaped octacosatungstate $[W_{28}O_{94}H_2]^{18-}$ moiety observed in the $[Ln_4(H_2O)_{22}W_{28}O_{94}H_2]^{6-}$ subunit is composed of two undecatungstate $[W_{11}O_{38}H]^{9-}$ fragments joined through a hexatungstate $[W_6O_{22}]^{8-}$ fragment by sharing four μ_2-O atoms. In **4**, 22-isopolytungstate $[W_{22}O_{74}H_2]^{14-}$ anions are interlinked together by four W–O–Eu1–O–W linkers giving rise to the 1-D chain motif, and then adjacent 1-D chains are further bridged through multiple W–O–Eu2–O–W connectors to engender the two-dimensional extended sheet structure with the 4-connected topology. The isomorphic **5**–**10** demonstrate the discrete structure consisting of a $[Ln(H_2O)_4][Ln(H_2O)_5]_2[W_{22}O_{74}H_2]^{8-}$ unit. The pH ranges in which **3**, **4**, and **9** are stable in aqueous solution have been examined by virtue of UV and ESI–MS spectra. The solid-state luminescent properties of **3**, **4**, and **6** have been probed at room temperature. **3** displays the pink emission derived from characteristic emission bands of the Sm^{3+} cations that correspond to transitions from the $^4G_{5/2}$ excited-state to lower ^6H_J (J = 5/2, 7/2, 9/2, 11/2) levels, **4** emits the red light that mainly results from the $^5D_0 \rightarrow {}^7F_2$ transition of the Eu^{3+} cations, and **6** manifests the green luminescence mainly originating from the $^5D_4 \rightarrow {}^7F_5$ transition of the Tb^{3+} cations. Their lifetime decay curves all conform to the single exponential function, affording their lifetimes of 8094.19 ns, 149.00 μs and 384.89 μs, respectively.

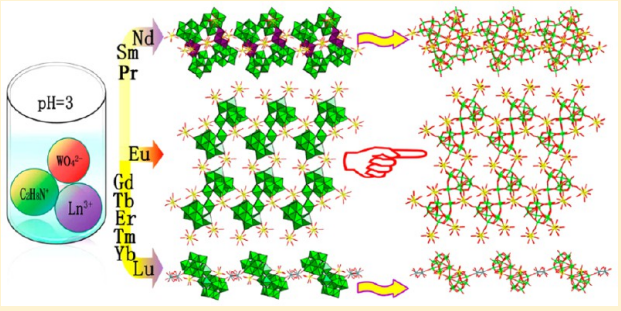

INTRODUCTION

Polyoxometalates (POMs), as a family of emblematic anionic metal–oxygen clusters, have attracted a high level of attention not only because of their structural and functional diversities, but also owing to their potential applications in catalysis, medicine, magnetism, gas sorption, electronic materials, and nonlinear optics.[1−5] From the viewpoint of the chemical compositions, POMs are usually constructed by early transition-metals (TMs) in their highest oxidation states, most of which commonly comprise Mo^{VI}, W^{VI}, V^V, and Nb^V.[6−10]

Within the POM field, it is well-known that polyoxotungstates (POTs) are the largest and most important subfamily. According to the discrepancy of components, POTs are usually categorized into two main types: heteropolyoxotungstates (hetero-POTs) and isopolyoxotungstates (iso-POTs). Hetero-POTs are written with the general formula $[X_pW_qO_y]^{n-}$ in which X represents the heteroatoms (e.g., P^V, Si^{IV}, Ge^{IV}, As^V).[11] Researchers are familiar with some typical structures such as the Wells–Dawson or Dawson-like $[X_pW_{18}O_y]^{n-}$ (p = 1 or 2, y = 60 or 62) and Keggin $[XW_{12}O_{40}]^{n-}$ anions.[12−14] Hitherto, a great quantity of hetero-POTs have emerged and have been reported. Compared with abundant hetero-POTs, investigations on iso-POTs with the

Received: July 14, 2015
Revised: November 13, 2015
Published: November 24, 2015

DOI: 10.1021/acs.cgd.5b00996
Cryst. Growth Des. 2016, 16, 108−120

general formula $[W_qO_y]^{n-}$ have garnered much less attention, which may be presumably related to the lack of the internal heteroatoms in iso-POTs that can help to stabilize the POM structures and the more labile and unstable nature of isopolyoxotungstate building blocks in comparison with hetero-POTs.[15] Even if the number of iso-POTs is not as high as that of hetero-POTs, some examples of iso-POTs were discovered. For example, in 2008, Cronin et al. communicated the inorganic crown ether analogue $[H_{12}W_{36}O_{120}]^{12-}$,[16] and two iso-POTs $[H_4W_{22}O_{74}]^{12-}$ and $[H_{10}W_{34}O_{116}]^{18-}$.[17] In addition, preparation and search of TM-containing iso-POTs (TM-iso-POTs) are also a crucial domain and have received considerable attention. Furthermore, some achievements have been made such as Fang's tetradeca-manganese aggregate $[Mn_{14}W_{48}O_{192}H_{20}]^{26-}$,[18] and Cronin's gigantic cluster $\{W_{200}Co_8O_{660}\}$.[19] In contrast to TM-iso-POTs, Ln-containing iso-POTs (Ln-iso-POTs) are another concerned branch due to their interesting properties in the areas of luminescence, catalysis, electrochemistry, and magnetism.[20] Some representative examples are as follows: Peacock and Weakley synthesized the first series of sandwich-type decatungstate species $[Ln(W_5O_{18})_2]^{n-}$ in a solution of pH 6.5−7.5.[21,22] Later, some $[Ln(W_5O_{18})_2]^{n-}$ structures with different alkali cations were also published by Yamase's group.[23−25] These discoveries merely are seen as a starting point in the domain of Ln-iso-POTs. In the past 10 years, some interesting and novel Ln-iso-POTs have been successively prepared. For instance, Cao et al. reported a special Ce-iso-POT $[H_6Ce_2(H_2O)ClW_{15}O_{54}]^{7-}$ fabricated by triangular $\{W_5O_{18}\}$ units capped by two cerium ions accompanying a terminal aqua ligand on one side and a terminal chloro ligand on the other side.[26] Kortz et al. addressed a class of Ln-iso-POTs based on docosatungstate fragments and a type of V-shaped Ln-iso-POTs including octacosatungstate segments.[27,28] Niu and co-workers synthesized Ln-containing peroxoisopolyoxotungstates involving the $[W_7O_{22}(O_2)_2]^{6-}$ units with a tetrahedral WO_4^{2-} template core.[29] Su et al. communicated a family of Ce^{3+}-iso-POT nanoclusters via pH-controlling assembly.[30]

Considering that the area of iso-POTs is still in its infancy, as a result, searching and discovering novel Ln-iso-POTs have gradually been developed as a significant research domain with the profound development of POM chemistry. Recently, our group has launched investigations on novel Ln-iso-POTs with interesting structures and properties by the self-assembly reaction of simple tungstates with Ln^{3+} cations in the participation of organic solubilizers using the conventional aqueous solution approach. Such a one-step strategy is convenient and unnecessary to prepare POT precursors and can shorten the experimental process. Fortunately, some fruitful findings have been harvested by us. For example, two types of unique oxalate-connective Ln-iso-POTs $Na_{10}[Ln_2(C_2O_4)(H_2O)_4(OH)W_4O_{16}]_2\cdot 30H_2O$ and $K_4Na_{16}[Ln(C_2O_4)W_5O_{18}]_4\cdot 60H_2O$ (Ln = Eu^{3+}, Ho^{3+}, Er^{3+}, Tb^{3+}) were obtained in a pH = 6.5−7.8 solution in 2014.[31] Notably, these two structure types can be controlled by the type of alkaline metal cations; that is, $Na_{10}[Ln_2(C_2O_4)(H_2O)_4(OH)W_4O_{16}]_2\cdot 30H_2O$ can be acquired only in the presence of Na^+ ions, while $K_4Na_{16}[Ln(C_2O_4)W_5O_{18}]_4\cdot 60H_2O$ can be isolated in the attendance of mixed Na^+ and K^+ ions.[31] Summarizing and comparing the previously reported Ln-iso-POTs, it is noteworthy that those Ln-iso-POTs with extended structures are much less developed. On the other hand, during the course of our exploration on novel Ln-containing POMs, we have found that the internal nature of Ln^{3+} ions (one crucial reason may be lanthanide contraction) has an important influence on the structures of target products.[31,32] For example, in the process of preparing the Cu−Ln heterometallic germanotungstates, the early Ln^{3+} (La^{3+}, Pr^{3+}) ions led to the tetrameric architecture $\{Cu(en)_2[Ln(\alpha\text{-}GeW_{11}O_{39})_2]_2\}^{24-}$, while the middle Ln^{3+} (Eu^{3+}, Tb^{3+}, Dy^{3+}) ions resulted in the dimeric motif $\{[Cu_3Ln(en)_3(OH)_3(H_2O)_2](\alpha\text{-}GeW_{11}O_{39})\}_2^{4-}$.[32] When we synthesized two types of unique oxalate-connective Ln-iso-POTs,[31] we also observed that only the middle and late Ln ions can form this two structural types. However, when the early Ln^{3+} cations were used in this system, the Peacock and Weakley's $[Ln(W_5O_{18})_2]^{n-}$ analogues were obtained.[21] These findings encourage us to continueously explore the Ln-controlling assembly of POTs and probe the effect of the internal nature of Ln^{3+} ions on the structural variety of Ln-iso-POTs. In the current work, we will introduce dimethylamine hydrochloride (DMAHC) as the organic solubilizer to improve the reaction capacity of the system of $Na_2WO_4\cdot 2H_2O$ and $Ln(NO_3)_3\cdot 6H_2O$ in aqueous acidic medium. A large number of our experiments have revealed that the introduction of DMAHC into the system can effectively reduce the possibility of forming the precipitations derived from the combination of in situ generated iso-POT fragments and Ln^{3+} cations. Furthermore, the capacity that the WO_4^{2-} anion can polymerize to various iso-POT building blocks in the aqueous solution has been extensively cognized by reported results;[17−31] thus, these facts make it possible that versatile and oxyphilic Ln^{3+} cations can integrate in situ generated iso-POT fragments together into large aggregates or even extended frameworks. On the basis of the above considerations, three types of Ln-iso-POTs $[H_2N(CH_3)_2]_6Na_6[Ln_4(H_2O)_{22}W_{28}O_{94}H_2]_2\cdot 113H_2O$ [Ln = Pr^{3+} (**1**), Nd^{3+} (**2**), Sm^{3+} (**3**)], Na_2 $[Eu(H_2O)_7]_2[Eu(H_2O)_5]_2[W_{22}O_{74}H_2]\cdot 20H_2O$ (**4**), and $Na_3H_2[Ln(H_2O)_4][Ln(H_2O)_5]_2[W_{22}O_{74}H_2]\cdot 36H_2O$ [Ln = Gd^{3+} (**5**), Tb^{3+} (**6**), Er^{3+} (**7**), Tm^{3+} (**8**), Yb^{3+} (**9**), Lu^{3+} (**10**)] have been successfully obtained under the aqueous solution condition, which are also characterized by elemental analyses, IR spectra, TG analyses, and single crystal X-ray diffraction. Structural analyses demonstrate that the molecular structural units of **1**, **2**, and **3** contain a hexameric Ln_8-comprising $[Ln_4(H_2O)_{22}W_{28}O_{94}H_2]_2^{12-}$ cluster anion; what's more, adjacent $[Ln_4(H_2O)_{22}W_{28}O_{94}H_2]_2^{12-}$ cluster anions are further combined together by means of $[Ln(H_2O)_5]^{3+}$ junctures, propagating a 1-D infinite chain structure. To the best of our knowledge, **1**−**3** stand for the first 1-D infinite chain based on Ln_8-comprising $[Ln_4(H_2O)_{22}W_{28}O_{94}H_2]_2^{12-}$ cluster anions. **4** is the first 2-D sheet architecture with a 4-connected topology established by 22-isopolytungstate $[W_{22}O_{74}H_2]^{14-}$ anions via Eu^{3+} linkers. The structures of **5**−**10** are discrete, and each contains a $[Ln(H_2O)_4][Ln(H_2O)_5]_2[W_{22}O_{74}H_2]^{8-}$ unit. Experimental results display that the synergistic effect of the nature of Ln^{3+} ions and the pH variation in the reaction process affect the structural diversity of **1**−**10**. To investigate their stability in aqueous solution with different pH values, UV spectra of **3**, **4**, and **9** in the acid and alkali range have been elaborately explored. Furthermore, the solid-state luminescence properties and their lifetime decay curves of **3**, **4**, and **6** have been measured at room temperature and are discussed in detail.

EXPERIMENTAL SECTION

Materials and Methods. All purchased chemicals were used without further purification. Carbon, nitrogen, and hydrogen analyses were obtained on a Perkin−Elmer 2400−II CHNS/O analyzer. Inductively coupled plasma atomic emission spectrometry (ICP-AES) was measured on a Perkin−Elmer Optima 2000 ICP-AES spectrometer.

DOI: 10.1021/acs.cgd.5b00996
Cryst. Growth Des. 2016, 16, 108−120

Table 1. Crystallographic Data and Structure Refinements for 1−10

	1	2	3	4	5
empirical formula	$C_{12}H_{366}N_6Na_6O_{345}Pr_8W_{56}$	$C_{12}H_{366}N_6Na_6O_{345}Nd_8W_{56}$	$C_{12}H_{366}N_6Na_6O_{345}Sm_8W_{56}$	$H_{92}Eu_4Na_2O_{118}W_{22}$	$H_{104}Na_3O_{124}Gd_3W_{22}$
formula weight	17677.93	17704.57	17753.45	6679.26	6674.25
crystal system	triclinic	triclinic	triclinic	triclinic	triclinic
space group	$P\bar{1}$	$P\bar{1}$	$P\bar{1}$	$P\bar{1}$	$P\bar{1}$
a, Å	19.176(2)	19.101(2)	18.967(6)	13.314(4)	12.5945(15)
b, Å	21.784(3)	21.822(2)	21.604(6)	13.823(4)	13.6605(17)
c, Å	21.988(3)	22.016(3)	21.774(7)	18.671(6))	17.290(2)
α, deg	70.774(2)	70.682(2)	70.704(6)	72.470(5)	90.852(2)
β, deg	69.672(2)	69.699(2)	69.801(5)	82.580(5)	101.817(2)
γ, deg	85.916(2)	85.648(2)	85.824(6)	61.497(4)	112.923(2)
V, Å^{-3}	8122.9(18)	8114.3(16)	7894(4)	2879.0(15)	2667.0(6)
Z	1	1	1	1	1
μ, mm^{-1}	21.042	21.143	21.904	24.137	25.593
F(000)	7922	7930	7946	2938	2949
T, K	296(2)	296(2)	296(2)	296(2)	296(2)
limiting indices	$-22 \le h \le 22$	$-22 \le h \le 22$	$-22 \le h \le 22$	$-15 \le h \le 15$	$-14 \le h \le 14$
	$-19 \le k \le 25$	$-24 \le k \le 25$	$-24 \le k \le 25$	$-16 \le k \le 15$	$-16 \le k \le 9$
	$-25 \le l \le 26$	$-26 \le l \le 23$	$-25 \le l \le 21$	$-22 \le l \le 21$	$-20 \le l \le 20$
no. of reflections collected	41975	41909	41029	14635	13431
no. of independent reflections	28425	28315	27582	9986	9156
R_{int}	0.0407	0.0674	0.0698	0.0461	0.0324
data/restrains/parameters	28425/40/1435	28315/118/1460	27582/117/1446	9986/24/592	9156/25/569
goodness-of-fit on F^2	1.047	1.008	1.021	1.079	1.041
final R indices [$I > 2\sigma(I)$]	$R_1 = 0.0528$	$R_1 = 0.0649$	$R_1 = 0.0645$	$R_1 = 0.0496$	$R_1 = 0.0503$
	$wR_2 = 0.1415$	$wR_2 = 0.1145$	$wR_2 = 0.1120$	$wR_2 = 0.1363$	$wR_2 = 0.1253$
R indices (all data)	$R_1 = 0.0834$	$R_1 = 0.1355$	$R_1 = 0.1310$	$R_1 = 0.0592$	$R_1 = 0.0601$
	$wR_2 = 0.1637$	$wR_2 = 0.1303$	$wR_2 = 0.1278$	$wR_2 = 0.1420$	$wR_2 = 0.1298$

	6	7	8	9	10
empirical formula	$H_{104}Na_3O_{124}Tb_3W_{22}$	$H_{104}Na_3O_{124}Er_3W_{22}$	$H_{104}Na_3O_{124}Tm_3W_{22}$	$H_{104}Na_3O_{124}Yb_3W_{22}$	$H_{104}Na_3O_{124}Lu_3W_{22}$
formula weight	6679.26	6704.28	6709.29	6721.62	6727.19
crystal system	triclinic	triclinic	triclinic	triclinic	triclinic
space group	$P\bar{1}$	$P\bar{1}$	$P\bar{1}$	$P\bar{1}$	$P\bar{1}$
a, Å	12.5675(8)	12.5583(9)	12.5850(9)	12.5431(19)	12.5601(9)
b, Å	13.6241(8)	13.6654(10)	13.6621(10)	13.659(2)	13.6777(10)
c, Å	17.2729(10)	17.2344(12)	17.2898(12)	17.213(3	17.2054(13)
α, deg	90.9330(10)	90.9890(10)	90.9500(10)	91.028(2)	90.9810(10)
β, deg	101.8210(10)	101.6110(10)	101.7550(10)	101.566(2)	101.5200(10)
γ, deg	112.8680(10)	113.0660(10)	112.9200(10)	113.129(2)	113.1870(10)
V, Å^{-3}	2652.1(3)	2650.3(3)	2665.4(3)	2641.5(7)	2647.2(3)
Z	1	1	1	1	1
μ, mm^{-1}	25.860	26.251	26.238	26.611	26.702
F(000)	2952	2961	2964	2967	2969
T, K	296(2)	296(2)	296(2)	296(2)	296(2)
limiting indices	$-14 \le h \le 14$	$-14 \le h \le 14$	$-14 \le h \le 14$	$-14 \le h \le 14$	$-14 \le h \le 11$
	$-16 \le k \le 12$	$-16 \le k \le 12$	$-16 \le k \le 16$	$-11 \le k \le 16$	$-10 \le k \le 16$
	$-18 \le l \le 20$	$-19 \le l \le 20$	$-20 \le l \le 15$	$-20 \le l \le 19$	$-20 \le l \le 19$
no. of reflections collected	13636	13545	13596	13050	13437
no. of independent reflections	9276	9209	9252	9009	9161
R_{int}	0.0303	0.0338	0.0438	0.0509	0.0367
data/restrains/parameters	9276/7/569	9209/48/569	9252/55/563	9009/126/563	9161/42/571
goodness-of-fit on F^2	1.046	1.005	1.031	1.035	1.015
final R indices [$I > 2\sigma(I)$]	$R_1 = 0.0408$	$R_1 = 0.0470$	$R_1 = 0.0573$	$R_1 = 0.0686$	$R_1 = 0.0469$
	$wR_2 = 0.1111$	$wR_2 = 0.1175$	$wR_2 = 0.1373$	$wR_2 = 0.1851$	$wR_2 = 0.1225$
R indices (all data)	$R_1 = 0.0498$	$R_1 = 0.0624$	$R_1 = 0.0786$	$R_1 = 0.0783$	$R_1 = 0.0580$
	$wR_2 = 0.1173$	$wR_2 = 0.1236$	$wR_2 = 0.1462$	$wR_2 = 0.1917$	$wR_2 = 0.1282$

IR spectra were recorded from solid samples pelletized with KBr on a Nicolet 170 SXFT−IR spectrometer in the range of 400−4000 cm^{-1}. UV spectra were performed with a U-4100 spectrometer at room temperature. Photoluminescence spectra and lifetime were carried out on an Edinburgh FLS 980 analytical instrument equipped with a 450 W xenon lamp and a μF900H high-energy microsecond flashlamp as the

DOI: 10.1021/acs.cgd.5b00996
Cryst. Growth Des. 2016, 16, 108−120

excitation source. Powder X-ray diffraction (PXRD) patterns were collected on a Bruker D8 ADVANCE instrument with Cu Kα radiation (λ = 1.54056 Å). Electrospray ionization mass spectrometry (ESI-MS) was performed on a Bruker Micro TOF-QII instrument. TG analyses were performed under a N_2 atmosphere on a Mettler−Toledo TGA/SDTA 851^e instrument with a heating rate of 10 °C min^{-1} from 25 to 700 °C.

Synthesis of $[H_2N(CH_3)_2]_6Na_6[Pr_4(H_2O)_{22}W_{28}O_{94}H_2]_2\cdot 113H_2O$ (1). $Na_2WO_4\cdot 2H_2O$ (1.00 g, 3.07 mmol) and DMAHC (0.50 g, 6.13 mmol) were dissolved in 40 mL of distilled water with stirring, and the pH of the solution was adjusted to 3.0 by HCl (6 mol·L^{-1}). After the solution was stirred for around 30 min, then $Pr(NO_3)_3\cdot 6H_2O$ (0.15 g, 0.34 mmol) was added into the solution. After the pH value was adjusted to 3.0 again, the solution was stirred for another 30 min and then filtered. Slow evaporation of the filtrate at the ambient temperature resulted in the light green needle crystals of **1** in about 1 week. Yield: 0.17 g (22.7%) based on $Pr(NO_3)_3\cdot 6H_2O$. Elemental analysis (%) calcd: H, 2.09; C, 0.82; N, 0.48; Na, 0.78; Pr, 6.38; W, 58.24. Found: H, 2.18; C, 0.97; N, 0.62; Na, 0.84; Pr, 6.46; W, 58.05. IR (KBr, cm^{-1}): 3409(s), 3176(w), 2788(w), 1629(m), 1460(m), 1402(w), 948(m), 823(s), 631(s), 426(w).

Synthesis of $[H_2N(CH_3)_2]_6Na_6[Nd_4(H_2O)_{22}W_{28}O_{94}H_2]_2\cdot 113\ H_2O$ (2). The synthesis process of **2** is similar to **1** except that $Pr(NO_3)_3\cdot 6H_2O$ (0.15 g, 0.34 mmol) was replaced by $Nd(NO_3)_3\cdot 6\ H_2O$ (0.15 g, 0.34 mmol). Pale purple needle crystals of **2** were afforded. Yield: 0.20 g (26.5%) based on $Nd(NO_3)_3\cdot 6H_2O$. Elemental analysis (%) calcd: H, 2.08; C, 0.81; N, 0.47; Na, 0.78; Nd, 6.51; W, 58.15. Found: H, 2.21; C, 0.99; N, 0.55; Na, 0.88; Nd, 6.34; W, 57.97. IR (KBr, cm^{-1}): 3407(s), 3175(w), 2789(w), 1628(m), 1465(m), 1401(w), 948(m), 820(s), 629(s), 430(w).

Synthesis of $[H_2N(CH_3)_2]_6Na_6[Sm_4(H_2O)_{22}W_{28}O_{94}H_2]_2\cdot 113\ H_2O$ (3). The synthesis process of **3** is similar to **1** except that $Nd(NO_3)_3\cdot 6H_2O$ (0.15 g, 0.34 mmol) was replaced by $Sm(NO_3)_3\cdot 6\ H_2O$ (0.15 g, 0.34 mmol). The light yellow needle crystals of **3** were formed. Yield: 0.23 g (30.5%) based on $Sm(NO_3)_3\cdot 6H_2O$. Elemental analysis (%) calcd: H, 2.08; C, 0.81; N, 0.47; Na, 0.78; Sm, 6.78; W, 57.99. Found: H, 2.25; C, 0.94; N, 0.54; Na, 0.85; Sm, 6.56; W, 57.82. IR (KBr, cm^{-1}): 3407(s), 3173(w), 2783(w), 1622(m), 1459(m), 1401(w), 948(m), 818(s), 629(s), 424(w).

Synthesis of $Na_2[Eu(H_2O)_7]_2[Eu(H_2O)_5]_2[W_{22}O_{74}H_2]\cdot 20\ H_2O$ (4). **4** was prepared by following the same procedure as **1** except that $Eu(NO_3)_3\cdot 6H_2O$ (0.15 g, 0.34 mmol) replaced $Nd(NO_3)_3\cdot 6\ H_2O$ (0.15 g, 0.34 mmol). The colorless needle crystals of **4** were obtained. Yield: 0.18 g (31.7%) based on $Eu(NO_3)_3\cdot 6H_2O$. Elemental analysis (%) calcd: H, 1.39; Na, 0.69; Eu, 9.10; W, 60.56. Found: H, 1.50; Na, 0.59; Eu, 8.90; W, 59.95. IR (KBr, cm^{-1}): 3392(s), 3165(w), 2762(w), 1622(m), 1459(m), 1401(w), 941(s), 814(s), 701(s), 502(w), 424(w).

Synthesis of $Na_3H_2[Gd(H_2O)_4][Gd(H_2O)_5]_2[W_{22}O_{74}H_2]\cdot 36H_2O$ (5). The synthesis process of **5** is similar to **1** except that $Nd(NO_3)_3\cdot 6\ H_2O$ (0.15 g, 0.34 mmol) was replaced by $Gd(NO_3)_3\cdot 6H_2O$ (0.15 g, 0.33 mmol). The colorless needle crystals of **5** were isolated. Yield: 0.25 g (34.2%) based on $Gd(NO_3)_3\cdot 6H_2O$. Elemental analysis (%) calcd: H, 1.57; Na, 1.03; Gd, 7.07; W, 60.60. Found: H, 1.72; Na, 0.94; Gd, 7.36; W, 60.83. IR (KBr, cm^{-1}): 3399(s), 3159(w), 2783(w), 1629(m), 1469(m), 1401(w), 940(s), 814(s), 693(s), 502 (w), 430 (w).

Synthesis of $Na_3H_2[Tb(H_2O)_4][Tb(H_2O)_5]_2[W_{22}O_{74}H_2]\cdot 36H_2O$ (6). The synthesis process of **6** is similar to **1** except that $Nd(NO_3)_3\cdot 6\ H_2O$ (0.15 g, 0.34 mmol) was replaced by $Tb(NO_3)_3\cdot 6H_2O$ (0.15 g, 0.33 mmol). The colorless needle crystals of **6** were isolated. Yield: 0.23 g (31.3%) based on $Tb(NO_3)_3\cdot 6H_2O$. Elemental analysis (%) calcd: H, 1.57; Na, 1.03; Tb, 7.14; W, 60.56. Found: H, 1.75; Na, 0.92; Tb, 7.42; W, 60.70. IR (KBr, cm^{-1}): 3406(s), 3151(w), 2789(w), 1628(m), 1459(m), 1401(w), 941(s), 814(s), 693(s), 502 (w), 430 (w).

Synthesis of $Na_3H_2[Er(H_2O)_4][Er(H_2O)_5]_2[W_{22}O_{74}H_2]\cdot 36H_2O$ (7). The synthesis process of **7** is similar to **1** except that $Nd(NO_3)_3\cdot 6\ H_2O$ (0.15 g, 0.34 mmol) was replaced by $Er(NO_3)_3\cdot 6H_2O$ (0.15 g, 0.33 mmol). The pink needle crystals of **7** were isolated. Yield: 0.21g (28.5%) based on $Er(NO_3)_3\cdot 6H_2O$. Elemental analysis (%) calcd: H, 1.56; Na, 1.03; Er, 7.48; W, 60.33. Found: H, 1.78; Na, 0.90; Er, 7.75; W, 60.45. IR (KBr, cm^{-1}): 3399(s), 3158(w), 2789(w), 1628(m), 1469(m), 1401(w), 941(s), 814(s), 689(s), 503 (w), 431 (w).

Synthesis of $Na_3H_2[Tm(H_2O)_4][Tm(H_2O)_5]_2[W_{22}O_{74}H_2]\cdot 36H_2O$ (8). The synthesis process of **8** is similar to **1** except that $Nd(NO_3)_3\cdot 6\ H_2O$ (0.15 g, 0.34 mmol) was replaced by $Tm(NO_3)_3\cdot 6H_2O$ (0.15 g, 0.32 mmol). The colorless needle crystals of **8** were isolated. Yield: 0.24g (33.5%) based on $Tm(NO_3)_3\cdot 6H_2O$. Elemental analysis (%) calcd: H, 1.56; Na, 1.03; Tm, 7.55; W, 60.28. Found: H, 1.80; Na, 0.94; Tm, 7.72; W, 60.56. IR (KBr, cm^{-1}): 3399(s), 3159(w), 2785(w), 1629(m), 1469(m), 1401(w), 940(s), 814(s), 693(s), 502 (w), 430 (w).

Synthesis of $Na_3H_2[Yb(H_2O)_4][Yb(H_2O)_5]_2[W_{22}O_{74}H_2]\cdot 36H_2O$ (9). The synthesis process of **9** is similar to **1** except that $Nd(NO_3)_3\cdot 6\ H_2O$ (0.15 g, 0.34 mmol) was replaced by $Yb(NO_3)_3\cdot 6H_2O$ (0.15 g, 0.32 mmol). The colorless needle crystals of **9** were isolated. Yield: 0.17 g (23.7%) based on $Yb(NO_3)_3\cdot 6H_2O$. Elemental analysis (%) calcd: H, 1.56; Na, 1.03; Yb, 7.72; W, 60.17. Found: H, 1.79; Na, 0.89; Yb, 7.79; W, 60.57. IR (KBr, cm^{-1}): 3399(s), 3165(w), 2789(w), 1628(m), 1465(m), 1404(w), 941(s), 815(s), 692(s), 502(w), 431(w).

Synthesis of $Na_3H_2[Lu(H_2O)_4][Lu(H_2O)_5]_2[W_{22}O_{74}H_2]\cdot 36H_2O$ (10). The synthesis process of **10** is similar to **1** except that $Nd(NO_3)_3\cdot 6\ H_2O$ (0.15 g, 0.34 mmol) was replaced by $Lu(NO_3)_3\cdot 6H_2O$ (0.15 g, 0.32 mmol). The colorless needle crystals of **10** were isolated. Yield: 0.15 g (20.9%) based on $Lu(NO_3)_3\cdot 6H_2O$. Elemental analysis (%) calcd: H, 1.56; Na, 1.03; Lu, 7.80; W, 60.12. Found: H, 1.82; Na, 0.94; Lu, 7.72; W, 60.49. IR (KBr, cm^{-1}): 3398(s), 3159(w), 2793(w), 1628(m), 1462(m), 1401(w), 941(s), 817(s), 695(s), 502 (w), 430 (w).

X-ray Crystallography. Single-crystal X-ray diffraction data for **1**−**10** were collected on a Bruker APEX−II CCD detector at 296(2) K with Mo Kα radiation (λ = 0.71073 Å). Direct methods were used to solve their structures and locate the heavy atoms using the SHELXTL-97 program package.[33,34] The remaining atoms were found from successive full-matrix least-squares refinements on F^2 and Fourier syntheses. Lorentz polarization and SADABS corrections were applied. All hydrogen atoms attached to carbon and nitrogen atoms were geometrically placed and refined isotropically as a riding model using the default SHELXTL parameters. No hydrogen atoms associated with water molecules were located from the difference Fourier map. All non-hydrogen atoms were refined anisotropically except for some sodium, oxygen, nitrogen, and carbon atoms and water molecules. The alert about low bond precision on C−C bonds in the checkcif report derives from shading of reciprocal space by the pressure cell, and it is unavoidable in high pressure crystal structure determinations. In the refinements, 48 lattice water molecules for **1**, 51 lattice water molecules for **2**, 48 lattice water molecules for **3**, and 17 lattice water molecules for **5**−**10** per molecule were found from the Fourier maps. However, there are still solvent accessible voids in the check cif reports of crystal structures, suggesting that some water molecules should exist in the structures that cannot be found from the weak residual electron peaks. These water molecules are highly disordered and attempts to locate and refine them were unsuccessful. On the basis of charge-balance considerations, elemental analyses, and TG analyses, 65 lattice water molecules for **1**, 62 lattice water molecules for **2**, 65 lattice water molecules for **3**, and 19 lattice water molecules for **5**−**10** were directly added to each molecular formula. The crystallographic data and structure refinement parameters for **1**−**10** are listed in Table 1. Crystallographic data for **1**, **2**, **3**, and **4**−**10** in this paper have been deposited in the Cambridge Crystallographic Data Centre with CCDC 1430481, 1411408, 1411409, and 1437596−1437602 for **1**, **2**, **3**, and **4**−**10**, respectively. These data can be obtained free of charge from The Cambridge Crystallographic Data Centre via www.ccdc.cam.ac.uk/data_request/cif.

RESULTS AND DISCUSSION

Synthesis. **1**−**10** were all synthesized by utilizing a one-pot reaction of $Na_2WO_4\cdot 2H_2O$, $Ln(NO_3)_3\cdot 6H_2O$, and DMAHC in aqueous acidic medium. The successful syntheses of **1**−**10** can be viewed as the assembly induced by the synergistic action of the nature of Ln^{3+} cations and the pH variation in the reaction

DOI: 10.1021/acs.cgd.5b00996
Cryst. Growth Des. 2016, 16, 108−120

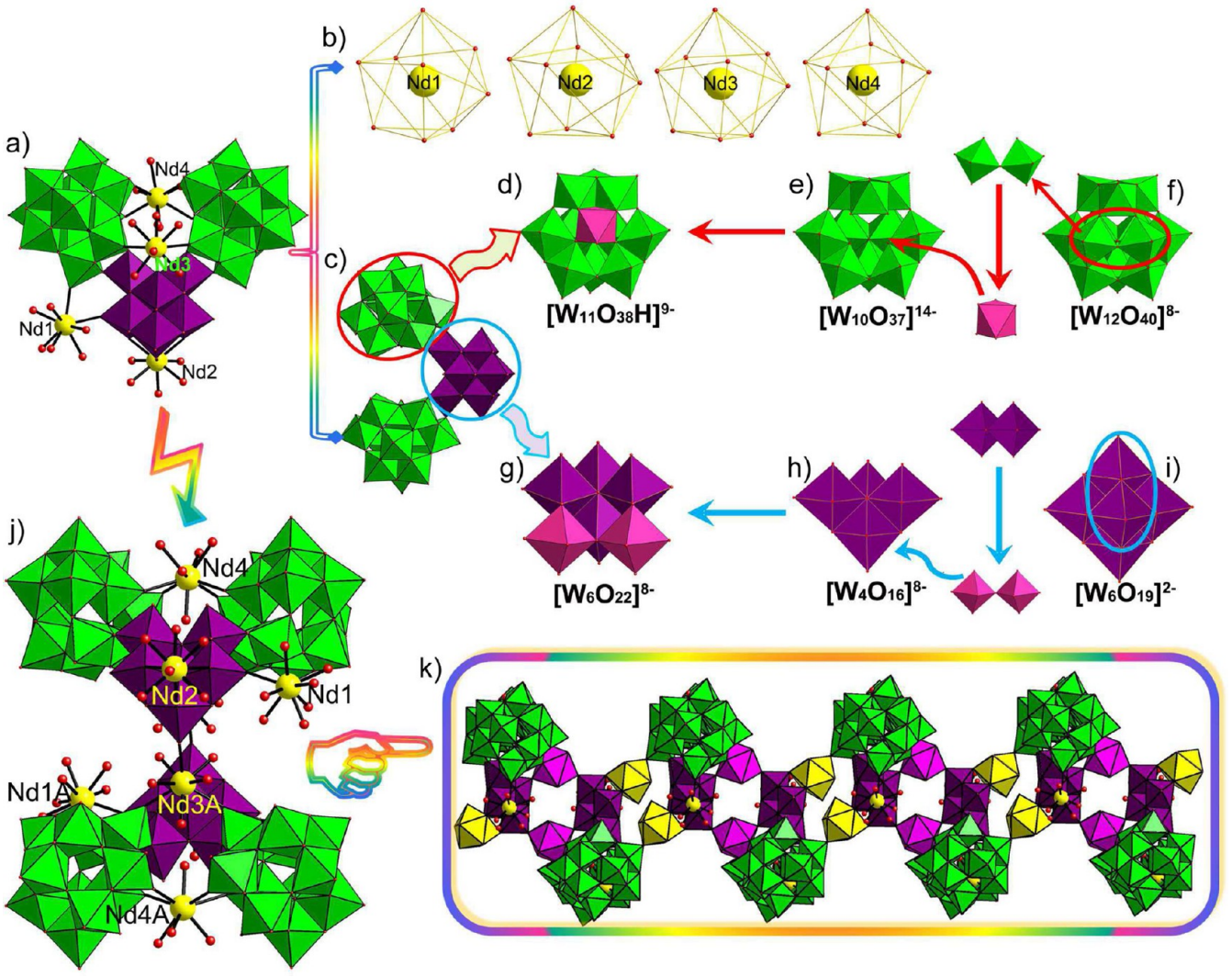

Figure 1. (a) The asymmetric $\{Nd_4W_{28}O_{94}\}$ subunit of **2**. (b) The monocapped square antiprismatic geometries of the $Nd1^{3+}$, $Nd2^{3+}$, $Nd3^{3+}$, $Nd4^{3+}$ ions. (c) The scare λ-shaped octacosatungstate $[W_{28}O_{94}H_2]^{18-}$ moiety. (d) The unusual undecatungstate $[W_{11}O_{38}H]^{9-}$ fragment. (e) The divacant Keggin $[W_{10}O_{37}]^{14-}$ segment. (f) The classical Keggin-like metatungstate $[\alpha\text{-}W_{12}O_{40}]^{8-}$ polyoxoanion. (g) The special hexatungstate $[W_6O_{22}]^{8-}$ fragment. (h) The Lindqvist divacant $[W_4O_{16}]^{8-}$ segment. (i) The well-known Lindqvist $[W_6O_{19}]^{2-}$ polyoxoanion. (j) The hexameric $\{Nd_8W_{56}O_{188}\}$ cluster anion. (k) The 1-D chain-like structure of **2** constructed from hexameric $\{Nd_8W_{56}O_{188}\}$ cluster anions through Nd^{3+} linkers. The atoms with the suffix A are generated by the symmetry operation (A: $2-x, -y, 1-z$).

process under the acidic conditions. During our exploration, we first used Pr^{3+}, Nd^{3+}, or Sm^{3+} cations to react with other simple materials giving rise to **1**, **2**, and **3**. Considering the influence of the nature of Ln^{3+} cations on the structures of products, we replaced Nd^{3+} and Sm^{3+} cations by utilizing other Ln^{3+} cations under the same conditions, and beyond our expectation, other two kinds of **4** and **5**−**10** were obtained. The results of parallel experiments reveal that different Ln^{3+} cations may result in the various products because the radius of Ln^{3+} cations has a vital effect on the construction of products. Similar phenomena have been also previously encountered.[35] In addition, the usage amount of Ln^{3+} cations is also an important factor in the reaction process. When the usage amount is changed from 0.15 to 0.25 g, **1**−**4** cannot be harvested, whereas **5**−**10** were still obtained even if the yield is very low. Apart from exploring the influence of Ln^{3+} cations in above aspects, great efforts were also put into the study of other conditions such as increasing the solubility of Ln^{3+} cations in the solution. Eventually, we observe that DMAHC can act as an organic solubilizer to increase the solubility of Ln^{3+} cations in the reaction solution. The reaction solution will become turbid in the absence of DMAHC. Therefore, DMAHC plays an important role in the system, although they are absent in the resulting products of **4**−**10**. Furthermore, the pH value is a significant factor as well in the reaction and has a great effect on the crystallization and structural construction of the products. A range of investigations indicate that the initial pH value of 2.9−3.2 is helpful for the formation of **1**−**10**, whereas their yields will be highest when the pH value is adjusted to 3.0 with keeping other conditions unchanged. On a close inspection of the pH variation in the reaction process of **1**−**10** (Table S1, Supporting Information), we find that the pH of the reaction system decreases to 2.57−2.66 for **1**−**3**, 2.67 for **4**, and 2.73−2.82 for **5**−**10** after 11 h. And then the pH almost remains unchanged. This fact suggests that the pH variation in the reaction process can affect the structural diversity of products.

Structural Description. The isostructural **1**−**3** are the first 1-D chain architecture assembled from Ln_8-containing $\{Ln_8W_{56}O_{188}\}$ units via $[Ln(H_2O)_5]^{3+}$ bridges, **4** illustrates the

DOI: 10.1021/acs.cgd.5b00996
Cryst. Growth Des. 2016, 16, 108−120

first 2-D extended sheet structure based on $[W_{22}O_{74}H_2]^{14-}$ anions, $[Eu(H_2O)_7]^{3+}$ cations and $[Eu(H_2O)_5]^{3+}$ cations, and **5**−**10** exhibit the 1-D chain architecture constructed from $\{[Ln(H_2O)_5]_2[W_{22}O_{74}H_2]\}^{8-}$ units via disordered $[Ln(H_2O)_4]^{3+}$ connectors. It should be pointed out that they all comprise the undecatungstate $[W_{11}O_{38}H]^{9-}$ fragment in their skeletons. Bond valence sum (BVS) calculations[36] of **2**, **4**, and **9** indicate that the oxidation states of all W and Ln atoms are +6 and +3, respectively (Tables S2−S4, Supporting Information). In order to determine the probable proton bonding positions, BVS values of all oxygen atoms on the POM skeletons of the symmetrical molecular units of **2**, **4**, and **9** have been calculated (Tables S2−S4, Supporting Information). The BVS values of O50 in **2**, O3 in **4**, and O2 in **9** are 1.184, 1.205, and 1.272, respectively, which are apparently lower than 2 and imply that these oxygen atoms are the most possible proton binding positions.

1, **2**, and **3** are isomorphous and both crystallize in the triclinic space group $P\bar{1}$ and illustrate a 1-D chain-like fashion constructed from Ln_8-containing $[Ln_4(H_2O)_{22}W_{28}O_{94}H_2]_2^{12-}$ $\{Ln_8W_{56}O_{188}\}$ units via Ln^{3+} bridges. Therefore, only the structure of **2** is described as an example. The molecular structural unit of **2** consists of 1 hexameric $[Nd_4(H_2O)_{22}W_{28}O_{94}H_2]_2^{12-}$ $\{Nd_8W_{56}O_{188}\}$ cluster anion, 6 dissociative $[H_2N(CH_3)_2]^+$ cations, 6 Na^+ cations, and 113 lattice water molecules. Interestingly, the centrosymmetric hexameric $\{Nd_8W_{56}O_{188}\}$ cluster anion can be viewed as fusion of two $[Nd_4(H_2O)_{22}W_{28}O_{94}H_2]^{6-}$ $\{Nd_4W_{28}O_{94}\}$ subunits by virtue of Nd_3^{3+} and Nd_3A^{3+} cations (A: $2-x$, $-y$, $1-z$) (Figure 1a). In the asymmetric $\{Nd_4W_{28}O_{94}\}$ subunit, there are four crystallographically unique Nd^{3+} cations (namely, $Nd1^{3+}$, $Nd2^{3+}$, $Nd3^{3+}$, $Nd4^{3+}$), which all adopt the nine-coordinate distorted monocapped square antiprismatic geometries (Figure 1b). It should be noted that the asymmetric $\{Nd_4W_{28}O_{94}\}$ subunit is established by a rare λ-shaped octacosatungstate $[W_{28}O_{94}H_2]^{18-}$ moiety (Figure 1c) with four supporting Nd^{3+} cations acting as one bidentate and three tetradentate ligands. One of the most remarkable features of **2** is that the λ-shaped octacosatungstate $[W_{28}O_{94}H_2]^{18-}$ moiety is composed of two undecatungstate $[W_{11}O_{38}H]^{9-}$ fragments (Figure 1d) linked via a hexatungstate $[W_6O_{22}]^{8-}$ fragment (Figure 1g) by sharing four μ_2-O atoms. To the best of our knowledge, such structural feature that one compound simultaneously includes two different types of iso-POT fragments is very rare.[28] On one hand, the undecatungstate $[W_{11}O_{38}H]^{9-}$ fragment, which is similar to $[H_4W_{11}O_{38}]^{6-}$ reported by Lehmann and Fuchs,[37] can be considered to be derived from the classical Keggin metatungstate $[\alpha\text{-}W_{12}O_{40}]^{8-}$ polyoxoanion (Figure 1f): two corner-sharing $\{WO_6\}$ octahedra located on the equatorial position are first removed away from the $[\alpha\text{-}H_2W_{12}O_{40}]^{6-}$ polyoxoanion, creating the divacant Keggin $[W_{10}O_{37}]^{14-}$ segment (Figure 1e), and then one $\{WO_6\}$ octahedron comes back to the vacant site and grafts to two $\{W_2O_{10}\}$ groups on the $[W_{10}O_{37}]^{14-}$ segment via two μ_3-O atoms and one $\{W_3O_{13}\}$ group on the $[W_{10}O_{37}]^{14-}$ segment via two μ_2-O and one μ_4-O atoms with accompanying the 60° rotation of the $\{W_3O_{13}\}$ triad located on the polar position, giving rise to the unusual undecatungstate $[W_{11}O_{38}H]^{9-}$ fragment (Figure 1d). This $[W_{11}O_{38}H]^{9-}$ fragment was also obtained by Niu et al. under solvothermal conditions in the preparation of a POM-based metal−organic framework $\{[Cu_2(bpy)(H_2O)_{5.5}]_2[W_{11}O_{38}\ H_2]\cdot 3H_2O\cdot 0.5CH_3CN\}$.[38] On the other hand, the special hexatungstate $[W_6O_{22}]^{8-}$ fragment, which was first observed by Lehmann and Fuchs in 1988,[37] can be looked at as resulting from the well-known Lindqvist $[W_6O_{19}]^{2-}$ polyoxoanion (Figure 1i): two edge-sharing $\{WO_6\}$ octahedra are taken away from the $[W_6O_{19}]^{2-}$ polyoxoanion, forming the divacant Lindqvist $[W_4O_{16}]^{8-}$ segment (Figure 1h), and then two edge-sharing $\{WO_6\}$ octahedra isomerize to two corner-sharing $\{WO_6\}$ octahedra, and eventually, two corner-sharing $\{WO_6\}$ octahedra link to the divacant $[W_4O_{16}]^{8-}$ segment via two μ_2-O and three μ_3-O atoms, constructing the hexatungstate $[W_6O_{22}]^{8-}$ fragment (Figure 1g). It is noteworthy that the C_s-symmetric $[W_6O_{22}]^{8-}$ fragment in **1**, **2**, and **3** is distinct from the C_i-symmetric $[W_6O_{22}]^{8-}$ fragment observed in $[C(NH_2)_3]_4[\{(CH_3)_2Sn\}_2(W_6O_{22})]\cdot 2H_2O$.[39] Alternatively, both types of $[W_6O_{22}]^{8-}$ fragments can be seen as the derivatives of the parent $[W_{10}O_{32}]^{4-}$ decametalate cluster.[40] The $[W_6O_{22}]^{8-}$ fragment in **1**, **2**, and **3** stems from the $[W_{10}O_{32}]^{4-}$ cluster by removing four $\{WO_6\}$ octahedra from the central part, whereas the $[W_6O_{22}]^{8-}$ fragment observed in $[C(NH_2)_3]_4[\{(CH_3)_2Sn\}_2(W_6O_{22})]\cdot 2H_2O$ is created by removal of two diagonally related pairs of $\{WO_6\}$ octahedra from the $[W_{10}O_{32}]^{4-}$ cluster.[39] In addition, albeit all the Nd^{3+} cations display the nine-coordinate monocapped square antiprismatic geometries, their coordination environments and the bridging functionalities are completely distinct in the construction of molecular structure. As shown in Figure 1j, the coordination sphere of the $Nd1^{3+}$ cation is completed by two terminal oxygen atoms and seven coordination water molecules with Nd−O distances of 2.44(2)−2.56(2) Å and the $Nd1^{3+}$ cation connects a $[W_{11}O_{38}H]^{9-}$ fragment and a $[W_6O_{22}]^{8-}$ fragment together through two terminal oxygen atoms. The coordination geometry of the $Nd2^{3+}$ cation is defined by three terminal oxygen atoms from a $[W_6O_{22}]^{8-}$ fragment, a terminal oxygen atom from a $[W_{11}O_{38}H]^{9-}$ fragment on a neighboring $\{Nd_8W_{56}O_{188}\}$ cluster anion and five water ligands with Nd−O distances of 2.449(17)−2.611(18) Å. The $Nd2^{3+}$ cations as connectors can join neighboring $\{Nd_8W_{56}O_{188}\}$ cluster anions together propagating a 1-D chain extended structure (Figure 1k), which is the other remarkable feature of **2**. As far as we know, such 1-D chain extended structure based on $\{Nd_8W_{56}O_{188}\}$ cluster anions is for the first time observed in POM chemistry. Different from the $Nd1^{3+}$ and $Nd2^{3+}$ cations, the monocapped square antiprism of the $Nd3^{3+}$ cation is constituted by four terminal oxygen atoms from two $[W_6O_{22}]^{8-}$ fragments and two $[W_{11}O_{38}H]^{9-}$ fragments and five water ligands with Nd−O distances of 2.450(17)−2.597(15) Å. The $Nd3^{3+}$ cation is first combined with two $[W_{11}O_{38}H]^{9-}$ fragments and one $[W_6O_{22}]^{8-}$ fragment in the asymmetric $\{Nd_4W_{28}O_{94}\}$ subunit, and then bridge two $\{Nd_4W_{28}O_{94}\}$ subunits together producing the hexameric $\{Nd_8W_{56}O_{188}\}$ cluster anion. Obviously, the $Nd2^{3+}$ cation plays an important role in the construction of the 1-D chain extended structure whereas the $Nd3^{3+}$ cation makes a significant contribution in the combination of two asymmetric $\{Nd_4W_{28}O_{94}\}$ subunits generating the hexameric $\{Nd_8W_{56}O_{188}\}$ cluster anion. The $Nd4^{3+}$ cation connects four terminal oxygen atoms from two $[W_{11}O_{38}H]^{9-}$ fragments and five water molecules to finish its nine-coordinate environment with Nd−O distances of 2.354(16)−2.720(15) Å.

In 2009, Kortz et al. communicated two 28-iso-POTs $[Ln_2(H_2O)_{10}W_{28}O_{92}(OH)_2]^{14-}$ (Ln = Sm^{III}, Eu^{III}) with discrete structures.[28] In spite of the above-mentioned examples, to certain degree, **1**, **2**, and **3** reported by us herein are still novel. The most remarkable differences lie in two aspects: (1) the structural units of **1**, **2**, and **3** consist of four crystallographically unique Ln^{3+} cations, while there are two crystallographically independent Ln^{3+} cations in $[Ln_2(H_2O)_{10}W_{28}O_{92}(OH)_2]^{14-}$; (2) **1**, **2**, and **3**

DOI: 10.1021/acs.cgd.5b00996
Cryst. Growth Des. 2016, 16, 108−120

exhibit a 1-D chain extended structure based on alternative $\{Ln_8W_{56}O_{188}\}$ cluster anions and Ln^{3+} cations linkers, on the contrary, $[Ln_2(H_2O)_{10}W_{28}O_{92}(OH)_2]^{14-}$ reported by Kortz et al. only forms the dimeric $\{Ln_4W_{56}\}$ cluster via the bridging role of Ln^{3+} cations. We conjecture that the appearance of much more Ln^{3+} centers in **1**, **2**, and **3** than that in $[Ln_2(H_2O)_{10}W_{28}O_{92}(OH)_2]^{14-}$ may be related to the fact that DMAHC can act as the organic solubilizer to increase the solubility of Ln^{3+} cations in the reaction solution.

4 also belongs to the triclinic space group $P\bar{1}$ and exhibits a 2-D sheet architecture. Its molecular structural unit is composed of a 22-iso-POT $[W_{22}O_{74}H_2]^{14-}$ anion (Figure 2a), two $[Eu(H_2O)_7]^{3+}$ cations, two $[Eu(H_2O)_5]^{3+}$ cations, two Na^+ cations, and 20 lattice water molecules. Different from the octacosatungstate $\{W_{28}\}$ moiety in **1**, **2**, and **3**, 22-isopolytungstate $[W_{22}O_{74}H_2]^{14-}$ anion in **4** can be visualized as a dimeric entity of two undecatungstate $[HW_{11}O_{38}]^{9-}$ subunits through two corner-sharing W−O−W bridges with the same W−O−W angle of 169.9°. This dimeric 22-iso-POT $[W_{22}O_{74}H_2]^{14-}$ anion has been observed by Kortz et al. in $[Ln_2(H_2O)_{10}W_{22}O_{72}(OH)_2]^{8-}$ (Ln = La^{III}, Ce^{III}, Tb^{III}, Dy^{III}, Ho^{III}, Er^{III}, Tm^{III}, Yb^{III}, Lu^{III}) in 2009.[27] Different from them, it is interesting that two crystallographically unique Eu^{3+} ($Eu1^{3+}$, $Eu2^{3+}$) cations are seen in **4** (Figure 2b,c). Albeit two types of Eu^{3+} cations display the nine-coordinate monocapped square antiprismatic geometries with the Eu−O distances of 2.402(11)−2.596(10) Å for the $Eu1^{3+}$ ion and 2.397(14)−2.58(4) Å for the $Eu2^{3+}$ cation, the distortions of their monocapped square antiprisms are different, which is relevant to the influence of the steric hindrance and their different coordination environments. The monocapped square antiprism of the $Eu1^{3+}$ cation is defined by three terminal atoms from one $[W_{22}O_{74}H_2]^{14-}$ anion, one terminal atom from the other $[W_{22}O_{74}H_2]^{14-}$ anion and five coordination water molecules. In contrast, the coordination sphere of the $Eu2^{3+}$ cation is completed by two terminal atoms from two neighboring $[W_{22}O_{74}H_2]^{14-}$ anions and seven water ligands. The most conspicuous characteristic of **4** is that contiguous 22-iso-POT $[W_{22}O_{74}H_2]^{14-}$ anions are interconnected together by four W−O−Eu1−O−W linkers giving rise to the 1-D chain motif (Figure 2d), and then adjacent 1-D chains are further joined through multiple W−O−Eu2−O−W connectors to engender the 2-D extended sheet structure (Figure 2e), for all we know, which stands for the first 2-D extended sheet constructed from $[W_{22}O_{74}H_2]^{14-}$ anions and Ln^{3+} cations. In the extended sheet, each $[W_{22}O_{74}H_2]^{14-}$anion is linked by eight Eu^{3+} cations, while each Eu^{3+} cation connects two $[W_{22}O_{74}H_2]^{14-}$ anions (Figure S1, Supporting Information), which is the other interesting architectural feature of **4**. Albeit the $[W_{22}O_{74}H_2]^{14-}$ anion own abundant oxygen atoms available to coordinate to Ln^{3+} cations, the eight-coordinate $[W_{22}O_{74}H_2]^{14-}$ anion observed in **4** is the highest coordinated $[W_{22}O_{74}H_2]^{14-}$ anion to date. From the viewpoint of topology, supposing that the molecular structural unit of **4** is considered as a four-connected node, the 2-D sheet of **4** manifests a 2-D (4,4)-network topology (Figure 2f).

5−**10** are also isomorphous and crystallize in the triclinic space group $P\bar{1}$ as well. Hence, **6** is taken as an example to be discussed in detail. As is shown in Figure 3a, the molecular unit of **6** is composed of one $[W_{22}O_{74}H_2]^{14-}$ anion, two types of crystallographically inequivalent Tb^{3+} cations, three Na^+ ions, two protons, and 36 water molecules of crystallization. In comparison with **4**, it is not difficult to discover that the $[W_{22}O_{74}H_2]^{14-}$ anions in **4** and **6** can be thought of as combination of two $[W_{11}O_{38}H]^{9-}$ subunits through two corner-sharing W−O−W

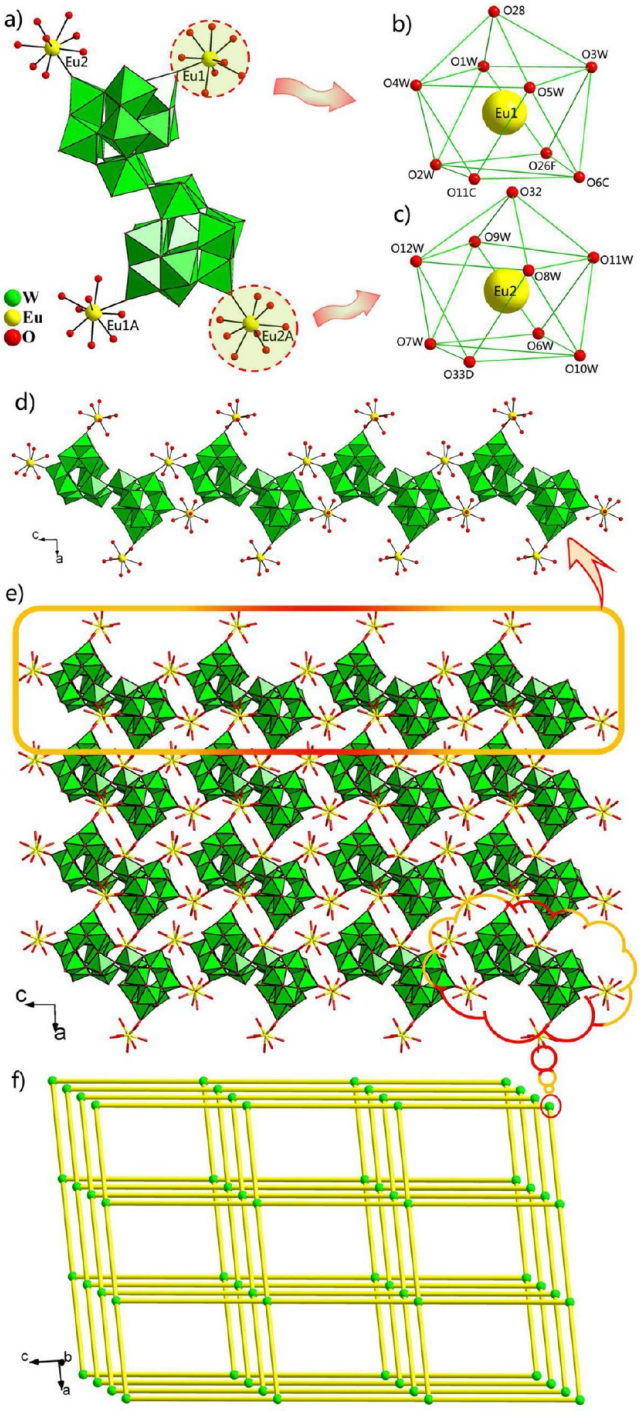

Figure 2. (a) Polyhedral and ball-and-stick view of the molecular structural unit of **4**. (b) The coordination environment of the $Eu1^{3+}$ cation. (c) The coordination environment of the $Eu2^{3+}$ cation. (d) The 1-D chain motif. (e) The 2-D sheet structure. (f) The 2-D (4,4) topological network. The lattice water molecules and protons are omitted for clarity. The atoms with the suffix "A−F" are generated by the symmetry operation where A: $-x, -y, 1-z$; B: $x, -1+y, 1+z$; C: $1-x, -y, 1-z$; D: $-x, 1-y, -z$; E: $-1+x, y, z$; F: $1+x, y, z$.

bridges. Distinct from **4**, $Tb1^{3+}$ and $Tb1A^{3+}$ cations in **6** are also used to link two $[W_{11}O_{38}H]^{9-}$ subunits (Figure 3d) together as well as the bridging role of two corner-sharing W−O−W linkers (Figure 3a,b). The $Tb1^{3+}$ ion is embedded in the eight-coordinate square antiprismatic geometry constituted by three terminal oxygen atoms from the $[W_{22}O_{74}H_2]^{14-}$ anion [Tb−O:

DOI: 10.1021/acs.cgd.5b00996
Cryst. Growth Des. 2016, 16, 108−120

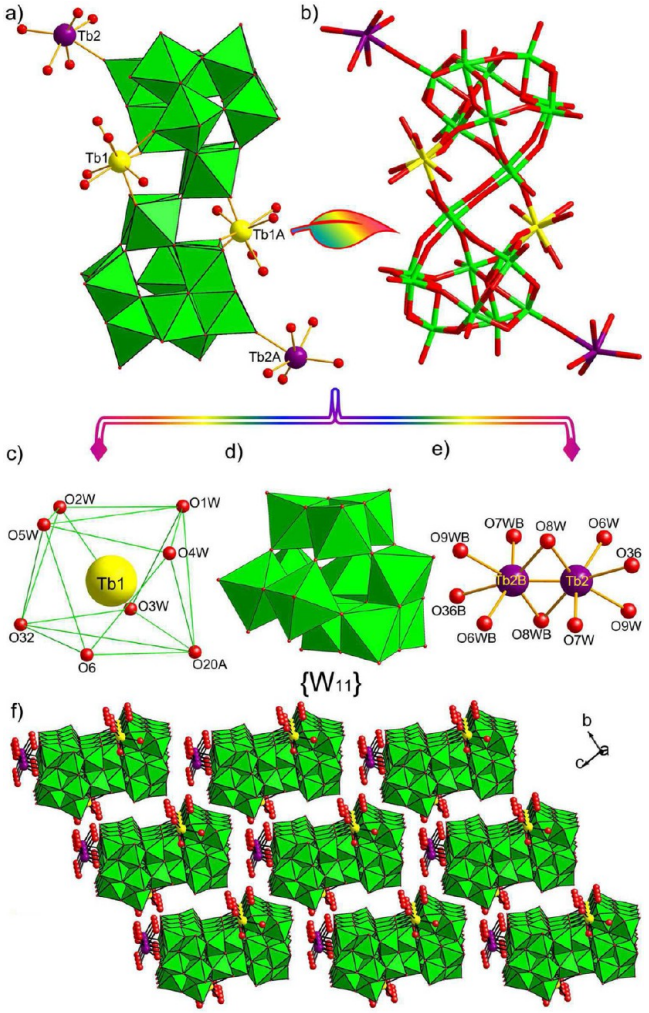

Figure 3. (a) The polyhedral and ball-and-stick representation of the molecular unit of **6**. (b) The wire representation of the molecular unit **6**. (c) The coordination environment of the $Tb1^{3+}$ cation. (d) The polyhedral view of the $[W_{11}O_{38}]^{10-}$ subunit. (e) The coordination environment of the disordered $Tb2^{3+}$ cation. (f) The 1-D chain-like structure of **6**. (g) The 3-D packing of $\{[Tb(H_2O)_4][Tb(H_2O)_5]_2[W_{22}O_{74}H_2]\}^{5-}$ units in **6** viewed along the *a* axis. The lattice water molecules and protons are omitted for clarity. The atoms with the suffix A, B are generated by the symmetry operation where A: $-2-x, -y, -z$; B: $-2-x, 1-y, 1-z$.

2.303(10)−2.416(9) Å] and five water ligands [Tb−O: 2.338(13)−2.453(12) Å] (Figure 3c). The $Tb2^{3+}$ cation coordinates to a terminal atom on the end of the $[W_{22}O_{74}H_2]^{14-}$ anion, while the $Tb2A^{3+}$ cation is symmetrically attached to a terminal atom on the other end of the $[W_{22}O_{74}H_2]^{14-}$ anion. Furthermore, the $Tb2^{3+}$ cation is disordered over two positions (Tb2 and Tb2B) with the site occupancy of 50% for each position (Figure 3e). This disordered phenomenon has been encountered in our previous research.[41] The $Tb2^{3+}$ cation exhibits a six-coordinate severely distorted octahedral geometry, which is made up of one oxygen atom from the $[W_{22}O_{74}H_2]^{14-}$ anion and five oxygen atoms from water molecules [Tb−O: 2.22(4)−2.51(5) Å]. Notably, because two disordered $Tb2^{3+}$ and $Tb2B^{3+}$ sites are never occupied simultaneously and the distance between adjacent 22-isopolytungstate fragments is too far to be connected by $[Tb_2(H_2O)_4]^{3+}$ cations, the structure of **6** is discrete. In the *bc* plane, the molecular $\{[Tb(H_2O)_4][Tb(H_2O)_5]_2[W_{22}O_{74}H_2]\}^{5-}$ units in **6** are regularly aligned in the −AAA− fashion. It is interesting that neighboring $\{[Tb(H_2O)_4][Tb(H_2O)_5]_2[W_{22}O_{74}H_2]\}^{5-}$ units along the *b* axis are distributed in the staggered pattern to reduce the steric hindrance (Figure 3f).

IR Spectra. IR spectra of **1**−**10** have been recorded between 4000 and 400 cm^{-1} on a Nicolet 170 SXFT−IR spectrometer by utilizing KBr pellets (Figure S2, Supporting Information). It is common sense for us that the broad and intense absorption band located in the range of 3407−3392 cm^{-1} originates from the ν(O−H) stretching mode of lattice or coordination water molecules and the absorption band centered at 1629−1633 cm^{-1} stems from the ν(O−H) bending vibration of the lattice or coordination water molecules.[31,42] Moreover, the existence of the iso-POT fragments in **1**−**10** was also elucidated by the features of their IR spectra. Their IR spectra demonstrate the characteristic vibration patterns derived from the W−O frameworks in the scope of 1000−650 cm^{-1}. In the case of **1**−**3**, the strong peak in 948 cm^{-1} can be assigned to the characteristic vibration band of the W═O bonds, whereas two groups of resonances between 820 and 629 cm^{-1} are deemed to the ν(W−O−W) stretching vibrations.[43] In a like manner, the strong absorption band at 941−940 cm^{-1} in **4**−**10** is attributed to the terminal W═O stretching vibration, and two groups of vibration signals appearing at 817−629 cm^{-1} are ascribed to the stretching vibration of the ν(W−O−W) bonds. In addition, the Ln−O stretching vibration of **4**−**10** is absent in the IR region, the possible reason for which is on account of the predominant ionic interactions between iso-POT units and Ln^{3+} cations.[44,45]

UV Spectra. Considering the fact that **1**, **2**, and **3** are isostructural, at the same time, **5**−**10** also are isomorphic, only UV and ESI−MS spectra of **3**, **4** and **9** as representatives were measured in the aqueous solution. First of all, in order to investigate the integrity of polyoxoanions of **3**, **4** and **9** when dissolving in water, their ESI−MS measurements have been carried out at room temperature. In the ESI−MS spectrum of **3**, the peak at *m*/*z* 3424.63 with the charge of −2 corresponds to the $\{H_{11}Na_5[W_{28}O_{94}H_2(H_2O)_4]\}^{2-}$ fragment (Figure S3, Supporting Information). In the ESI−MS spectrum of **4**, the peak at *m*/*z* 1143.79 with the charge of −5 is attributed to the $[Eu_3(W_{22}O_{74}H_2)\cdot 2H_2O]^{5-}$ fragment (Figure S4, Supporting Information). In the ESI-MS spectrum of **9**, the peak at *m*/*z* 1112.60 with the charge of −5 is assigned to the $[YbNa_3H_3(W_{22}O_{74}H_2)\cdot 5H_2O]^{5-}$ fragment (Figure S5, Supporting Information). It is obvious that some Ln^{3+} ions in **3**, **4**, and **9** depart from the polyoxoanion surfaces in the solution, further illustrating that the predominant ionic interactions between iso-POT anions and Ln^{3+} cations, which have been confirmed by the solid-state IR spectra. However, the iso-POT anions of **3**, **4** and **9** in the solution still remain integral, which offer the guarantee for probing the solution stability of them in different pH values. The UV spectra of **3**, **4** and **9** all display two absorption bands peaking at ca. 192 and 270 nm for **3**, ca. 194 and 285 nm for **4**, and ca. 192 and 285 nm for **9**, respectively (Figure S6, Supporting Information). The former energy absorption band can be attributed to the pπ−dπ charge-transfer transitions of the $O_t \rightarrow W$ (O_t was denoted as terminal oxygen atoms) bonds, whereas the latter energy absorption band is assigned to the pπ−dπ charge-transfer transitions of the $O_b \rightarrow W$ (O_b was denoted as bridging oxygen atoms) bonds.[46] As is known to all, POMs are extraordinarily sensitive to the pH of the studied medium. Hence, for the sake of investigating their stability in aqueous solution with different pH values, **3**, **4**, and **9** have been

DOI: 10.1021/acs.cgd.5b00996
Cryst. Growth Des. 2016, 16, 108−120

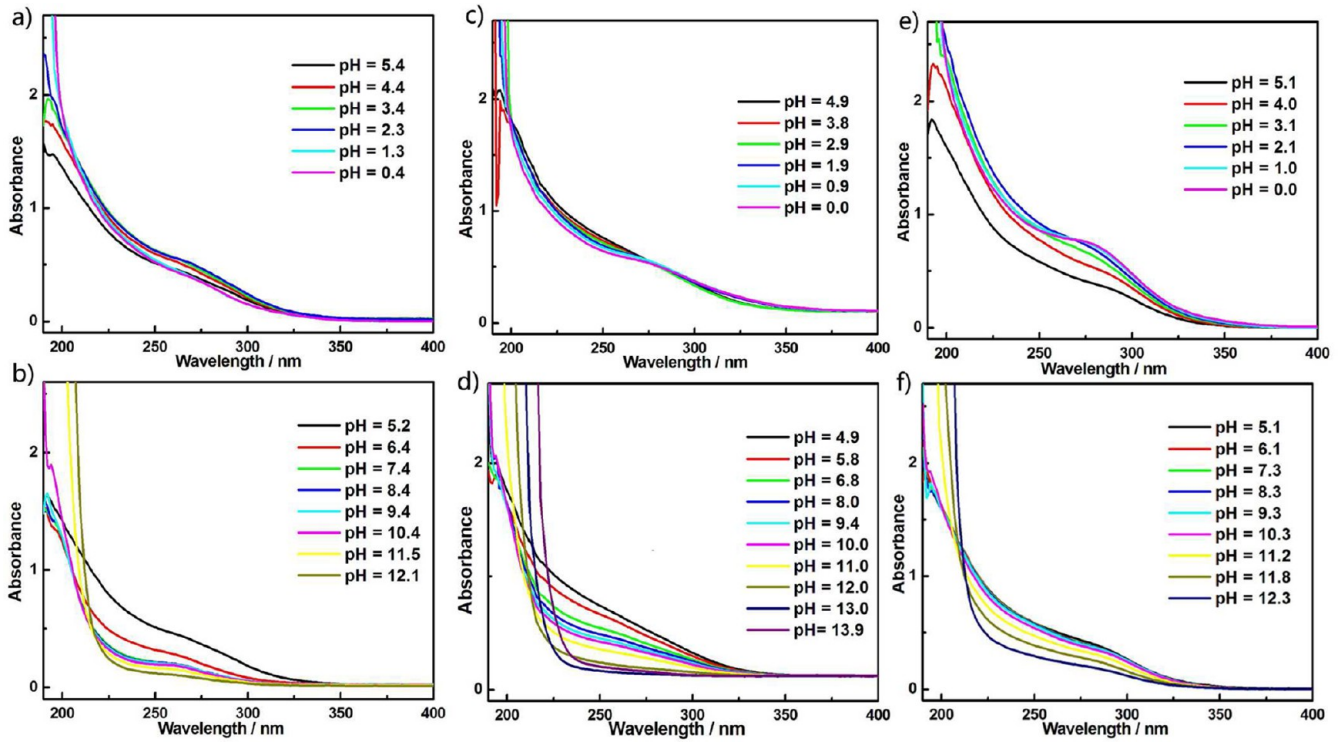

Figure 4. Influence of the pH values on the stability of **3**, **4**, **9** in aqueous solution: (a) The UV spectral evolution of **3** in acidic direction; (b) the UV spectral evolution of **3** in alkaline direction. (c) The UV spectral evolution of **4** in acidic direction. (d) The UV spectral evolution of **4** in alkaline direction. (e) The UV spectral evolution of **9** in acidic direction. (f) The UV spectral evolution of **9** in alkaline direction.

elaborately explored by taking advantage of UV spectra, which were measured in aqueous solution in the range of 400−190 nm. The pH in the alkaline direction and the acidic direction is adjusted by employing diluted NaOH and diluted H_2SO_4. When **3**, **4**, and **9** are dissolved in water, their solution pH values are 5.2, 4.9, and 5.1, respectively. As you can see from Figure 4a, when the pH gradually decreases near to 3.4, there is no obvious change of the UV spectrum of **3**. In contrast, in the alkaline direction, when the pH is higher than 7.4, both absorption bands gradually become weaker until they disappear (Figure 4b). In a short, **3** is stable in aqueous solution in the pH range of about 3.4−7.4. Similarly, as indicated in Figure 4c,d, **4** is stable in the pH range of ca. 3.8−6.8. The pH stable scope of **9** is ca. 4.1−7.3 (Figure 4e,f).

Photoluminescence Properties. Ln^{3+} elements have always played a prominent role in cathode ray tubes, tunable lasers, projection televisions, light-emitting diodes, fluorescent tubes, X-ray detectors, and efficient light conversion molecular devices.[47−49] Lately, in coordination chemistry, it has been learned that the peculiar luminescent properties of Ln^{3+}-based complexes are very promising for versatile applications in luminescent labels for fluoroimmunoassays, antennae for photosensitive bioinorganic compounds, amplifiers for optical communications and luminescence imaging for their high color purity and potentially high internal quantum efficiency.[50−52] Actually, some luminescent materials such as $BaMgAl_{10}O_{17}:Eu^{2+}$ and $GdMgB_5O_{10}:Ce^{3+},Tb^{3+}$ have been commercially used to blue and green luminescent lamps, respectively.[53] These particular functionalities are attributed to the narrow emission and high color purity originating from Ln^{3+} cations. In general, Ln^{3+} cations can be characterized by making use of a gradual filling of the 4f orbitals from $4f^0$ (for La^{3+}) to $4f^{14}$ (for Lu^{3+}). These electronic $[Xe]4f^n$ configurations (n = 0−14) can give rise to various electron energy levels that will lead to complicated optical characteristics.[54−56] Because their electron energy levels are well-defined owing to the good shielding of the 4f orbitals by the outer filled 5s and 5p subshells, Ln^{3+} cations are less sensitive to the chemical environments and still keep their atomic properties in Ln^{3+}-based complexes.[54] Therefore, each Ln^{3+} cation shows narrow and characteristic 4f−4f transitions, whereby the photoluminescence behaviors of the solid-state samples of **3**, **4**, and **6** have been investigated at room temperature. In order to identify the phase purity of **3**, **4**, and **6**, their PXRD patterns have been measured, and the consistency of the PXRD patterns of the bulks and the calculated patterns from the single-crystal structural analyses proves the good phase purity of **3**, **4**, and **6** (Figure S7, Supporting Information).

When **3** was excited under visible light of 402 nm, pink emission was observed with accompanying four characteristic luminescent emission bands with maxima at 560, 596, 642, and 706 nm in the photoluminescence spectrum (Figure 5a), which correspond to transitions from the $^4G_{5/2}$ excited-state to lower ^6H_J levels, namely, the $^4G_{5/2} \rightarrow {}^6H_{5/2}$ (560 nm), $^4G_{5/2} \rightarrow {}^6H_{7/2}$ (596 nm), $^4G_{5/2} \rightarrow {}^6H_{9/2}$ (642 nm), and $^4G_{5/2} \rightarrow {}^6H_{11/2}$ (706 nm) transitions.[57,58] The most intense peak is the transition $^4G_{5/2} \rightarrow {}^6H_{9/2}$ at 642 nm. By monitoring the $^4G_{5/2} \rightarrow {}^6H_{9/2}$ emission at 642 nm, the excitation spectrum of **3** was also collected (Figure 5b). The luminescent decay curve taken by monitoring the emission at 642 nm ($^4G_{5/2} \rightarrow {}^6H_{9/2}$) (Figure 5c) can be well fitted to a single exponential function as $I = A\exp(-t/\tau)$, affording the lifetime (τ) of 8094.2 ns, the pre-exponential factor (A) of 1111.83, and the agreement factor (χ^2) of 1.203. Under the excitation of UV light (395 nm), the emission spectrum of the as-synthesized solid of **4** consists of seven f−f transition lines within the Eu^{3+} $4f^6$ electron configuration (Figure 5d), which are assigned to the $^5D_1 \rightarrow {}^7F_1$ (537 nm), $^5D_1 \rightarrow {}^7F_2$ (556 nm), $^5D_0 \rightarrow {}^7F_0$ (578 nm), $^5D_0 \rightarrow {}^7F_1$ (593 nm), $^5D_0 \rightarrow {}^7F_2$

DOI: 10.1021/acs.cgd.5b00996
Cryst. Growth Des. 2016, 16, 108−120

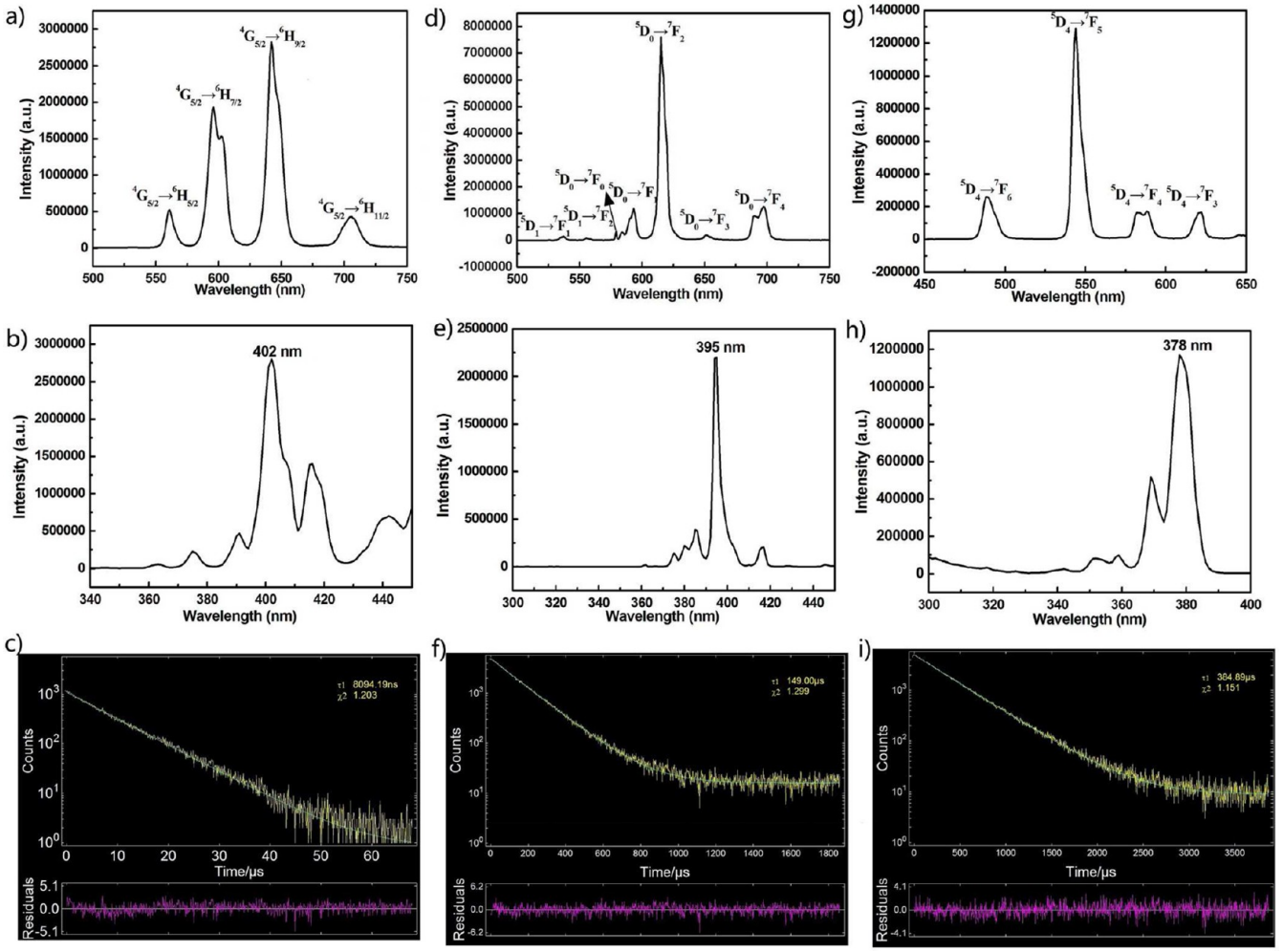

Figure 5. (a) The solid-state emission spectrum of **3** (λ_{ex} = 402 nm) at room temperature. (b) The solid-state excitation spectrum of **3** (λ_{em} = 642 nm). (c) The luminescence decay curve of **3** taken by monitoring the emission at 642 nm. (d) The solid-state emission spectrum of **4** (λ_{ex} = 395 nm) at room temperature. (e) The solid-state excitation spectrum of **4** (λ_{em} = 615 nm). (f) The luminescence decay curve of **4** taken by monitoring the emission at 615 nm. (g) The solid-state emission spectrum of **6** (λ_{ex} = 378 nm) at room temperature. (h) The solid-state excitation spectrum of **6** (λ_{em} = 543 nm). (i) The luminescence decay curve of **6** taken by monitoring the emission at 543 nm.

(615 nm), $^5D_0 \rightarrow {}^7F_3$ (662 nm), and $^5D_0 \rightarrow {}^7F_4$ (697 nm) transitions, respectively.[59,60] Generally speaking, the f−f transitions of the Ln^{3+} cation can be categorized to the parity allowed magnetic dipole transitions and the parity forbidden electric dipole transitions. Non-centrosymmetric chemical environments permit the mixing of electronic states of opposite parity into the 4f wave functions and the electric dipole transitions become partly allowed and the intensities of these transitions are especially sensitive to the change of the Ln^{3+} cation local environment; therefore, these transitions are normally known as "hypersensitive transitions".[53,55] Thus, the luminescence of Ln^{3+} cations is able to offer useful information on their local environments and functions as the structural probe to decipher the symmetry of the chemical environments and coordination spheres.[53] In this aspect, the luminescence of the Eu^{3+} cation can be work as a befitting structural probe to detect the coordination symmetry and even the number of aqueous ligands. In particular, the intensity ratio of the $^5D_0 \rightarrow {}^7F_2$/ $^5D_0 \rightarrow {}^7F_1$ transitions is extremely sensitive to the coordination symmetry of the Eu^{3+} cation and usually utilized as a criterion to evaluate the site symmetry of the Eu^{3+} cation,[61] because the magnetic-dipolar $^5D_0 \rightarrow {}^7F_1$ transition is less affected by the local environment whereas the electric-dipole $^5D_0 \rightarrow {}^7F_2$ transition is sensitive to the crystal field symmetry and heavily affected by the local environment. As a rule, the magnetic-dipole $^5D_0 \rightarrow {}^7F_1$ transition plays a dominant role in a centrosymmetric chemical environment, while the electronic-dipole $^5D_0 \rightarrow {}^7F_2$ transition is dominant in a noncentrosymmetric chemical environment.[62−67] The emission intensity ratio of the $^5D_0 \rightarrow {}^7F_2/{}^5D_0 \rightarrow {}^7F_1$ is 6.4 in the as-synthesized **4**, indicating the lower site symmetry of the Eu^{3+} cations, which coincides with the structure analysis results that two types of Eu^{3+} cations exhibit the nine-coordinate monocapped square antiprismatic geometries. Moreover, the symmetry-forbidden emission $^5D_0 \rightarrow {}^7F_0$ is seen 578 nm. This luminescence characteristic also consolidates that the Eu^{3+} cations dwell in the low symmetrical coordination environments.[53] Other else, theory shows that the dynamic coupling contribution can bear responsibility for this vast intensity variation of $^5D_0 \rightarrow {}^7F_2$ by the polarizability of the surrounding atoms, or groups of atoms.[48,66] Monitoring $Eu^{3+}{}^5D_0 \rightarrow {}^7F_2$ emission at 615 nm, the excitation spectrum has also been collected (Figure 5e). The excitation spectrum is dominated by a narrow line at 395 nm, which is attributable to the $^7F_0 \rightarrow {}^5L_6$ transition.[67] The $^5D_0$ lifetime curve of the Eu^{3+} ion was

DOI: 10.1021/acs.cgd.5b00996
Cryst. Growth Des. 2016, 16, 108−120

performed under the most intense emission at 615 nm and the excitation light at 395 nm (Figure 5f), which can also conform to a single exponential function, leading to the decay time of 149.0 μs, the pre-exponential factor of 4971.99, and the agreement factor (χ^2) of 1.299. The decay time for **4** is much shorter than those of the oxalate-connective Eu^{III}-substituted iso-POTs $Na_{10}[Eu_2(C_2O_4)(H_2O)_4(OH)W_4O_{16}]_2{\cdot}30H_2O$ (τ = 1.18 ms) and $K_4Na_{16}[Eu(C_2O_4)W_5O_{18}]_4{\cdot}60H_2O$ (τ = 1.20 ms) reported by us,[31] which can be ascribed to the fact that the aqua ligands on Eu^{3+} cations in **4** facilitate the radiationless deactivation of the $^5D_0$ state and partially quench the luminescence emission.[68] Analysis of the microstructure of **4** find that there are five or seven aqua coordination molecules are bonded to the Eu^{3+} cations, but each Eu^{3+} cation is combined with two aqua ligands in $Na_{10}[Eu_2(C_2O_4)(H_2O)_4(OH)W_4O_{16}]_2{\cdot}30H_2O$, and there is no aqua ligand on the Eu^{3+} cation in $K_4Na_{16}[Eu(C_2O_4)W_5O_{18}]_4{\cdot}60H_2O$. Hence, there is no doubt for the shorter luminescent lifetime of **4**. What's more, the lifetime of **4** is slightly longer than that (0.097 ms) of the Fe^{III}–Eu^{III} heterometallic tungstoantimonate $[Eu(H_2O)_8]_2[Fe_4(H_2O)_8(thr)_2][B\text{-}\beta\text{-}SbW_9O_{33}]_2{\cdot}22H_2O$ communicated by our group,[69] prevailingly because the number of aqua ligands on the Eu^{3+} cations in **4** is less than that of on the Eu^{3+} cations in $[Eu(H_2O)_8]_2[Fe_4(H_2O)_8(thr)_2][B\text{-}\beta\text{-}SbW_9O_{33}]_2{\cdot}22H_2O$. The solid-state sample of **6** emits the green luminescence upon excitation at 378 nm. Its emission spectrum displays four obvious characteristic emission peaks at 489 nm, 543 nm, 582 and 620 nm (Figure 5g), which are respectively attributed to the $^5D_4 \rightarrow {}^7F_6$, $^5D_4 \rightarrow {}^7F_5$, $^5D_4 \rightarrow {}^7F_4$, and $^5D_4 \rightarrow {}^7F_3$ transitions of the Tb^{3+} ions.[70] The excitation spectrum of **6** was also monitored under excitation at 378 nm and the most intense emission at 543 nm of the Tb^{III} cations (Figure 5h). The strong excitation band at 378 nm is derived from the $^7F_5 \rightarrow {}^5D_3$ transition of the Tb^{III} intra4f^8 ion.[71] The decay curve of **6** was also examined under the most intense emission at 543 nm and the excitation at 378 nm (Figure 5i), which can also be fitted into a single-exponential function, generating the lifetime of 384.89 μs, the pre-exponential factor of 4996.51, and the agreement factor (χ^2) of 1.151. In addition, as shown in Figure 6, the CIE chromaticity coordinates of the corresponding samples are (0.61378, 0.38520) for **3**, (0.65242, 0.34694) for **4**, and (0.33195, 0.59468) for **6**.

Thermal Properties. In order to examine the thermal stability and confirm the number of lattice water molecules of **1**–**10**, TG analyses have been performed on their crystalline samples under the flowing N_2 atmosphere from 25 to 700 °C with the heating rate of 10 °C min^{-1}. The TG curves of **1**–**10** show the one-step slow weight loss (Figures S8–S10, Supporting Information). **1**, **2**, and **3** display similar TG curves with a weight loss of 15.12% (calcd. 15.68%) for **1**, 15.33% (calcd. 15.62%) for **2**, and 14.77% (calcd. 15.57%) for **3**, which approximately correspond to the release of 113 lattice water molecules, 22 coordinate water molecules, and 6 dimethylamine molecules, and the dehydration of 10 protons. **4** also undergoes a one-step weight loss process with a weight loss of 12.40%, which is assigned to the loss of 20 lattice water molecules, 24 water ligands and the dehydration of two protons (calcd. 12.38%). The one-step weight loss of **5**–**10** is 13.44% (calcd. 14.03%) for **5**, 14.83% (calcd. 14.01%) for **6**, 14.15% (calcd. 13.96%) for **7**, 13.37% (calcd. 13.95%) for **8**, 13.36% (calcd. 13.93%) for **9**, and 13.32% (calcd. 13.91%) for **10**, respectively, which can be ascribed to the release of 36 lattice water molecules and 14 water ligands and the dehydration of four protons.

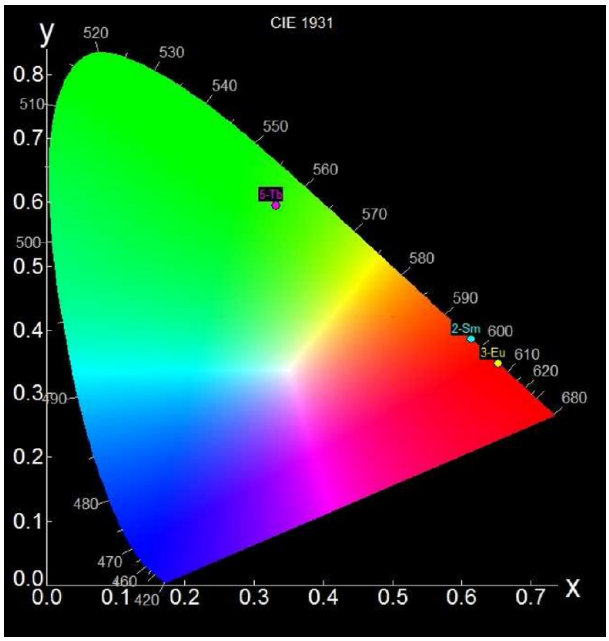

Figure 6. Corresponding color coordinates of **3**, **4**, and **6** under excitation at 402, 395, and 378 nm, respectively.

CONCLUSIONS

In conclusion, we have successfully prepared three kinds of Ln-iso-POTs $[H_2N(CH_3)_2]_6Na_6[Ln_4(H_2O)_{22}W_{28}O_{94}H_2]_2{\cdot}113H_2O$ [Ln = Pr^{3+} (**1**), Nd^{3+} (**2**), Sm^{3+} (**3**)], $Na_2[Eu(H_2O)_7]_2[Eu(H_2O)_5]_2[W_{22}O_{74}H_2]{\cdot}20H_2O$ (**4**), and $Na_3H_2[Ln(H_2O)_4][Ln(H_2O)_5]_2[W_{22}O_{74}H_2]{\cdot}36H_2O$ [Ln = Gd^{3+} (**5**), Tb^{3+} (**6**), Er^{3+} (**7**), Tm^{3+} (**8**), Yb^{3+} (**9**), Lu^{3+} (**10**)] by reaction of sodium tungstate and Ln^{3+} salts in the participation of DMAHC in the acidic aqueous medium. It is interesting that the synergistic effect of the nature of Ln^{3+} cations and the pH variation in the reaction process lead to the structural diversity of **1**–**10**. **1**, **2**, and **3** are the first 1-D chain structures made up of hexameric Ln_8-comprising $\{Nd_8W_{56}O_{188}\}$ entities and $[Ln(H_2O)_5]^{3+}$ connectors, in which the W_{56}-containing $\{Nd_8W_{56}O_{188}\}$ cluster anion is very unwonted. **4** manifests the first 2-D sheet architecture constituted by 22-isopolytungstate $[W_{22}O_{74}H_2]^{14-}$ moieties via Eu^{3+} linkers. The structures of **5**–**10** are discrete, and each consists of a $[Ln(H_2O)_4][Ln(H_2O)_5]_2[W_{22}O_{74}H_2]^{8-}$ unit. The solid-state photoluminescence spectrum of **3** exhibits four characteristic emission bands that are ascribed to $^4G_{5/2} \rightarrow {}^6H_J$ (J = 5/2, 7/2, 9/2, 11/2) transitions, **4** emits the red light that mainly results from the $^5D_0 \rightarrow {}^7F_2$ transition, and the green luminescence of **6** is majorly derived from the $^5D_4 \rightarrow {}^7F_5$ transition. Moreover, their lifetime decay curves all conform to the single exponential function [$I = A\exp(-t/\tau)$]. Apparently, our research findings about Ln-containing iso-POTs in this article together with our previous unique oxalate-connective Ln-substituted iso-POTs[31] will greatly extend the derivatization chemistry of Ln-incorporating iso-POTs. These diverse derivative functionalities mainly profits from the high coordination number and bridging role of oxyphilic Ln^{3+} cations and the flexible structural types of in situ formed iso-POT building blocks. These advantages in the Ln–iso-POT system will enlighten us to import polycarboxylate multifunctional groups to this system to explore much more novel organic–inorganic hybrid Ln-iso-POT materials with optical and magnetic properties.

DOI: 10.1021/acs.cgd.5b00996
Cryst. Growth Des. 2016, 16, 108–120

■ ASSOCIATED CONTENT

Supporting Information

The Supporting Information is available free of charge on the ACS Publications website at DOI: 10.1021/acs.cgd.5b00996.

BVS calculations of W, Ln, and O atoms in **2**, **4**, and **9**; IR spectra and related structural figures; ESI−MS spectra of **3**, **4**, and **9**; TG curves of **1**−**10** (PDF)

Accession Codes

CCDC 1411408−1411409, 1430481, and 1437596−1437602 contain the supplementary crystallographic data for this paper. These data can be obtained free of charge via www.ccdc.cam.ac.uk/data_request/cif, or by emailing data_request@ccdc.cam.ac.uk, or by contacting The Cambridge Crystallographic Data Centre, 12, Union Road, Cambridge CB2 1EZ, UK; fax: +44 1223 336033.

■ AUTHOR INFORMATION

Corresponding Authors

*(L.J. Chen) E-mail: ljchen@henu.edu.cn.

*(J.W. Zhao) E-mail: zhaojunwei@henu.edu.cn. Fax: (+86) 371 23886876.

Notes

The authors declare no competing financial interest.

■ ACKNOWLEDGMENTS

This work was supported by the Natural Science Foundation of China (21301049, U1304208, 21571048), Program for Science & Technology Innovation Talents in Universities of Henan Province, the Natural Science Foundation of Henan Province (122300410106, 142300410451), the Postdoctoral Foundation of Henan Province, 2014 Special Foundation for Scientific Research Project of Henan University, 2012 Young Backbone Teachers Foundation from Henan Province (2012GGJS-027) and the Students Innovative Pilot Plan of Henan University (2015). We also thank the assistance in discussion on electrospray ionization mass spectrometry from Dr. Chensong Pan at Bruker (Beijing) Scientific Technology Co. Ltd.

■ REFERENCES

(1) Marrot, J.; Pilette, M. A.; Haouas, M.; Floquet, S.; Taulelle, F.; Lopez, X.; Poblet, J. M.; Cadot, É. *J. Am. Chem. Soc.* **2012**, *134*, 1724.

(2) Zhao, Y.; Deng, D.-S.; Ma, L.-F.; Ji, B.-M.; Wang, L.-Y. *Chem. Commun.* **2013**, *49*, 10299.

(3) Heine, J.; Müller-Buschbaum, K. *Chem. Soc. Rev.* **2013**, *42*, 9232.

(4) Descalzo, A. B.; Martínez-Mañez, R.; Sancenon, F.; Hoffmann, K.; Rurack, K. *Angew. Chem., Int. Ed.* **2006**, *45*, 5924.

(5) Zheng, S.-T.; Zhang, J.; Li, X.-X.; Fang, W.-H.; Yang, G.-Y. *J. Am. Chem. Soc.* **2010**, *132*, 15102.

(6) Pope, M. T. *Heteropoly and Isopoly Oxometalates*; Springer: Berlin, 1983.

(7) Long, D. L.; Burkholder, E.; Cronin, L. *Chem. Soc. Rev.* **2007**, *36*, 105.

(8) Kortz, U.; Müller, A.; van Slageren, J.; Schnack, J.; Dalal, N. S.; Dressel, M. *Coord. Chem. Rev.* **2009**, *253*, 2315.

(9) Cronin, L.; Müller, A. *Chem. Soc. Rev.* **2012**, *41*, 7333.

(10) Zheng, S.-T.; Yang, G.-Y. *Chem. Soc. Rev.* **2012**, *41*, 7623.

(11) Ismail, A. H.; Bassil, B. S.; Suchopar, A.; Kortz, U. *Eur. J. Inorg. Chem.* **2009**, *2009*, 5247.

(12) Yin, P. C.; Li, T.; Forgan, R. S.; Lydon, C.; Zuo, X. B.; Zheng, Z. N.; Lee, B.; Long, D. L.; Cronin, L.; Liu, T. B. *J. Am. Chem. Soc.* **2013**, *135*, 13425.

(13) Ma, F. J.; Liu, S. X.; Sun, C. Y.; Liang, D. D.; Ren, G. J.; Wei, F.; Chen, Y. G.; Su, Z. M. *J. Am. Chem. Soc.* **2011**, *133*, 4178 (c).

(14) Streb, C.; Ritchie, C.; Long, D. L.; Kögerler, P.; Cronin, L. *Angew. Chem., Int. Ed.* **2007**, *46*, 7579.

(15) Long, D.-L.; Tsunashima, R.; Cronin, L. *Angew. Chem., Int. Ed.* **2010**, *49*, 1736.

(16) Streb, C.; McGlone, T.; Brücher, O.; Long, D.-L.; Cronin, L. *Chem. - Eur. J.* **2008**, *14*, 8861.

(17) Miras, H. N.; Yan, J.; Long, D.-L.; Cronin, L. *Angew. Chem., Int. Ed.* **2008**, *47*, 8420.

(18) Fang, X. K.; Luban, M. *Chem. Commun.* **2011**, *47*, 3066.

(19) De la Oliva, A. R.; Sans, V.; Miras, H. N.; Yan, J.; Zang, H. Y.; Richmond, C. J.; Long, D.-L.; Cronin, L. *Angew. Chem., Int. Ed.* **2012**, *51*, 12759.

(20) Ismail, A.; Dickman, M. H.; Kortz, U. *Inorg. Chem.* **2009**, *48*, 1559.

(21) Peacock, R. D.; Weakley, T. J. R. *J. Chem. Soc. A* **1971**, 1836.

(22) Iball, J.; Low, J. N.; Weakley, T. J. R. *J. Chem. Soc., Dalton Trans.* **1974**, 2021.

(23) Ozeki, T.; Takahashi, M. T.; Yamase, t. *Acta Crystallogr., Sect. C: Cryst. Struct. Commun.* **1992**, *48*, 1370.

(24) Ozeki, T.; Yamase, T. *Acta Crystallogr., Sect. C: Cryst. Struct. Commun.* **1993**, *49*, 1574.

(25) Ozeki, T.; Yamase, T. *Acta Crystallogr., Sect. C: Cryst. Struct. Commun.* **1994**, *50*, 327.

(26) Li, T. H.; Li, F.; Lü, J.; Guo, Z. G.; Gao, S. Y.; Cao, R. *Inorg. Chem.* **2008**, *47*, 5612.

(27) Ismail, A. H.; Dickman, M. H.; Kortz, U. *Inorg. Chem.* **2009**, *48*, 1559.

(28) Ismail, A. H.; Bassil, B. S.; Suchopar, A.; Kortz, U. *Eur. J. Inorg. Chem.* **2009**, *2009*, 5247.

(29) Song, L.-Y.; Zhang, D.-D.; Ma, P.-T.; Liang, Z.-J.; Wang, J.-P.; Niu, J.-Y. *CrystEngComm* **2013**, *15*, 4597.

(30) Chen, W.-C.; Wang, X.-L.; Jiao, Y.-Q.; Huang, P.; Zhou, E.-L.; Su, Z.-M.; Shao, K.-Z. *Inorg. Chem.* **2014**, *53*, 9486.

(31) Zhao, J. W.; Li, H. L.; Li, Y. Z.; Li, C. Y.; Wang, Z. L.; Chen, L. J. *Cryst. Growth Des.* **2014**, *14*, 5495.

(32) Zhao, J. W.; Shi, D. Y.; Chen, L. J.; Li, Y. Z.; Ma, P. T.; Wang, J. P.; Niu, J. Y. *Dalton Trans.* **2012**, *41*, 10740.

(33) Sheldrick, G. M. *SHELXS 97, Program for Crystal Structure Solution*; University of Göttingen: Göttingen, Germany, 1997.

(34) Sheldrick, G. M. *SHELXL 97, Program for Crystal Structure Refinement*; University of Göttingen: Germany, 1997.

(35) Nohra, B.; Mialane, P.; Dolbecq, A.; Riviere, E.; Marrot, J.; Sècheresse, F. *Chem. Commun.* **2009**, 2703.

(36) Brown, I. D.; Altermatt, D. *Acta Crystallogr., Sect. B: Struct. Sci.* **1985**, *41*, 244.

(37) Lehmann, T.; Fuchs, J. Z. Z. *Z. Naturforsch., B: J. Chem. Sci.* **1988**, *43*, 89.

(38) Han, Q. X.; Sun, X. P.; Li, J.; Ma, P. T.; Niu, J. Y. *Inorg. Chem.* **2014**, *53*, 6107.

(39) Reinoso, S.; Dickman, M. H.; Kortz, U. *Inorg. Chem.* **2006**, *45*, 10422.

(40) Swallow, A. G.; Barnes, W. H. *J. Am. Chem. Soc.* **1964**, *86*, 4209.

(41) Chen, L. J.; Zhang, F.; Ma, X.; Luo, J.; Zhao, J. W. *Dalton Trans.* **2015**, *44*, 12598.

(42) Szeto, K. C.; Lillerud, K. P.; Tilset, M.; Bjørgen, M.; Prestipino, C.; Zecchina, A.; Lamberti, C.; Bordiga, S. *J. Phys. Chem. B* **2006**, *110*, 21509.

(43) Sarma, M.; Chatterjee, T.; Das, S. K. *Dalton Trans.* **2011**, *40*, 2954.

(44) Auwer, C. D.; Charbonnel, M. C.; Drew, M. G. B.; Grigoriev, M.; Hudson, M. J.; Iveson, B. P.; Madic, C.; Nierlich, M.; Presson, M. T.; Revel, R.; Russell, M. L.; Thuery, P. *Inorg. Chem.* **2000**, *39*, 1487.

(45) Zhang, S. W.; Zhao, J. W.; Ma, P. T.; Niu, J. Y.; Wang, J. P. *Chem. - Asian J.* **2012**, *7*, 966.

(46) Niu, J. Y.; Wang, K. H.; Chen, H. N.; Zhao, J. W.; Ma, P. T.; Wang, J. P.; Li, M. X.; Bai, Y.; Dang, D. B. *Cryst. Growth Des.* **2009**, *9*, 4362.

(47) Armelao, L.; Quici, S.; Barigelletti, F.; Accorsi, G.; Bottaro, G.; Cavazzini, M.; Tondello, E. *Coord. Chem. Rev.* **2010**, *254*, 487.

(48) Rocha, J.; Carlos, L. D.; Paz, F. A. A.; Ananias, D. *Chem. Soc. Rev.* **2011**, *40*, 926.

DOI: 10.1021/acs.cgd.5b00996
Cryst. Growth Des. 2016, 16, 108−120

(49) Carlos, L. D.; Sá Ferreira, R. A.; Bermudez, V. de Z.; Ribeiro, S. J. L. *Adv. Mater.* **2009**, *21*, 509.
(50) Li, Y.; Zheng, F. K.; Liu, X.; Zou, W. Q.; Guo, C.; Lu, C. Z.; Huang, J. S. *Inorg. Chem.* **2006**, *45*, 6308.
(51) Bünzli, J. C. G.; Piguet, C. *Chem. Soc. Rev.* **2005**, *34*, 1048.
(52) Binnemans, K. *Chem. Rev.* **2009**, *109*, 4283.
(53) Cui, Y. J.; Yue, Y. F.; Qian, G. D.; Chen, B. L. *Chem. Rev.* **2012**, *112*, 1126.
(54) Moore, E. G.; Samuel, A. P. S.; Raymond, K. N. *Acc. Chem. Res.* **2009**, *42*, 542.
(55) Bünzli, J.-C. G. *Chem. Rev.* **2010**, *110*, 2729.
(56) Sopasis, G. J.; Orfanoudaki, M.; Zarmpas, P.; Philippidis, A.; Siczek, M.; Lis, T.; O'Brien, J. R.; Milios, C. J. *Inorg. Chem.* **2012**, *51*, 1170.
(57) Comby, S.; Scopelliti, R.; Imbert, D.; Charbonnière, L.; Ziessel, R.; Bunzli, J. G. *Inorg. Chem.* **2006**, *45*, 3158.
(58) Huang, Y.-G.; Wu, B.-L.; Yuan, D.-Q.; Xu, Y.-Q.; Jiang, F.-L.; Hong, M.-C. *Inorg. Chem.* **2007**, *46*, 1171.
(59) Xia, J.; Zhao, B.; Wang, H.-S.; Shi, W.; Ma, Y.; Song, H.-B.; Cheng, P.; Liao, D.-Z.; Yan, S.-P. *Inorg. Chem.* **2007**, *46*, 3450.
(60) Zhao, J. W.; Luo, J.; Chen, L. J.; Yuan, J.; Li, H. Y.; Ma, P. T.; Wang, J. P.; Niu, J. Y. *CrystEngComm* **2012**, *14*, 7981.
(61) Zhang, T.; Spitz, C.; Antonietti, M.; Faul, C. F. J. *Chem. - Eur. J.* **2005**, *11*, 1001.
(62) Kirby, A. F.; Richardson, F. S. *J. Phys. Chem.* **1983**, *87*, 2544.
(63) Stouwdam, J. W.; van Veggel, F. C. J. M. *Nano Lett.* **2002**, *2*, 733.
(64) Su, Y.; Li, L.; Li, G. *Chem. Mater.* **2008**, *20*, 6060.
(65) Xu, Q. H.; Li, L. S.; Liu, X. S.; Xu, R. R. *Chem. Mater.* **2002**, *14*, 549.
(66) Malta, O. L.; Carlos, L. D. *Quim. Nova* **2003**, *26*, 889.
(67) Hungerford, G.; Suhling, K.; Green, M. *Photochem. Photobiol. Sci.* **2008**, *7*, 734.
(68) Beeby, A.; Clarkson, I. M.; Dickins, R. S.; Faulkner, S.; Parker, D.; Royle, L.; deSousa, A. S.; Williams, J. A. G.; Woods, M. *J. Chem. Soc., Perkin Trans. 2* **1999**, *2*, 493.
(69) Zhao, J.-W.; Cao, J.; Li, Y.-Z.; Zhang, J.; Chen, L.-J. *Cryst. Growth Des.* **2014**, *14*, 6217.
(70) Sun, L.; Li, Y.; Liang, Z.-Q.; Yu, J.; Xu, R.-R. *Dalton Trans.* **2012**, *41*, 12790.
(71) Li, X.; Sun, H.-L.; Wu, X.-S.; Qiu, X.; Du, M. *Inorg. Chem.* **2010**, *49*, 1865.

DOI: 10.1021/acs.cgd.5b00996
Cryst. Growth Des. 2016, 16, 108−120